UNIVERSITY OF LEEDS

Article:
Abbas,, SZ, Dupont, V orcid.org/0000-0002-3750-0266 and Mahmud, T (2017) Modelling of high purity H2 production via sorption enhanced chemical looping steam reforming of methane in a packed bed reactor. Fuel, 202. pp. 271-286. ISSN 0016-2361

https://doi.org/10.1016/j.fuel.2017.03.072

Accepted in Fuel 23/03/2017

Modelling of high purity H_2 production via sorption enhanced chemical looping steam reforming of methane in a packed bed reactor

S. Z. Abbas*, V. Dupont, T. Mahmud

School of Chemical and Process Engineering, The University of Leeds, LS2 9JT, UK

ABSTRACT

Sorption enhanced chemical looping steam reforming of methane (SE-CLSR) relies on the exothermicity of both a metal catalyst's oxidation and the in situ CO_2 capture by carbonation onto a solid sorbent to provide the heat demand of hydrogen (H_2) production by steam reforming while generating a nearly pure H_2 product. A brief thermodynamic analysis to study the main features of the SE-CLSR process is done prior to the reactor modelling work. Later, one dimensional mathematical model of SE-CLSR process in the packed bed configuration is developed using gPROMS model builder 4.1.0® under the adiabatic conditions. This model combines reduction of the NiO catalyst with the steam reforming reactions, followed by the oxidation of the Ni-based reduced catalyst. The individual models of NiO reduction, steam reforming with in situ CO_2 capture on Ca-sorbent, and Ni re-oxidation are developed by using kinetic data available in literature and validated against previous published work. The model of SE-CLSR is then applied to simulate 10 alternative cycles of the fuel and air feed in the reactor. The performance of the model is studied in terms of CH_4 conversion, CO_2 capture efficiency, purity and yield of H_2. The sensitivity of the process is studied under the various operating conditions of temperature, pressure, molar steam to carbon ratio (S/C) and mass flux of the gas phase. In this work, the operating conditions used for the production of H_2 represent realistic industrial production conditions.The sensitivity analysis demonstrates that the developed model of SE-CLSR

process has the flexibility to simulate a wide range of operating conditions of temperature, pressure, S/C and mass flux of the gas phase.

Keywords: Modelling; Steam reforming; Chemical looping; CO_2 capture; Nickel catalyst

*Corresponding Author

Tel.: +44-7451919251

E-mail address: pmsza@leeds.ac.uk

1. Introduction

The linear trend of increase in temperature of the land shows that the average rise of 0.85°C is observed over the period of 1880 to 2012[1]. The researchers blamed CO_2 as the major cause of the global warming. The major contribution of CO_2 in the atmosphere is due to the burning of fossil fuel in the thermal power plants and heavy chemical industries such as petrochemical and fertilizer. It contributed to about 78% of total greenhouse gases (GHGs) emission from 1970 to 2010[2]**.**Increasing energy demands, depletion of fossil fuel reserves and pollution threats make H_2 an attractive alternative energy carrier. H_2 is widely considered as the fuel of the future and it has the capability to fuel the generation of electricity without emitting harmful pollutants. Currently, the maximum amount of H_2 is coming from natural gas (48%) followed by petroleum (30%), coal (18%) and electrolysis process (4%) [3].

The conventional steam methane reforming (SMR) process is the most widely used technique for H_2 production and over 50% of the world's H_2 production is from the SMR process[4]. The higher degree of endothermicity of the process makes it operate at high temperature conditions. In industrial SMR processes, water gas shift reactors are needed downstream of the reformer to convert the undesired CO into $CO_2$and H_2 product. Later on, amine scrubbing or pressure swing adsorption (PSA) process is required to achieve the higher purity of H_2[5]. To address the issue of global warming, researchers developed the concept of combining the

reforming process with in-situ CO_2 separation. This process was named sorption enhanced steam methane reforming (SE-SMR) process [5-7]. The addition of sorbent (CO_2 acceptor) along with the catalyst promotes the performance of the reforming process not only by shifting the reactions towards more H_2 production but also in terms of purity of H_2 (CO_2 free product), as well as suppressing equilibrium solid carbon by-product and permitting both lower temperatures of operations and steam demand[8].

The H_2 yield depends upon the type of CO_2 acceptor used. The selection of CO_2 acceptor depends upon its CO_2 capturing capacity, stability after multi-cycles of operation and on adequate sorption/desorption kinetics [9]. Calcium oxide (CaO) is found to be the best acceptor of CO_2 and resulted in 99% H_2 purity[10, 11]. CaO is a low cost sorbent and is considered as the most prominent sorbent for the CO_2 sorption under the reforming conditions. CaO shows good capacity of CO_2 capturing, good thermodynamic properties and good kinetics as compared to the other sorbents such as Li_2ZrO_3, $KLiZrO_3$, Li_4SiO_4 and Na_2ZrO_3. Spanish dolomite and calcite are good sorbents as well and they show very high capacity for CO_2 adsorption [12]. Stability of the CO_2 carrying capacity of the CaO is a key issue for the fixed-bed sorption enhanced technology, and it has to be confirmed for thousands of cycles. A drop of the re-carbonation extent for a pure CaO in re-carbonation/decomposition cycles is well-recognized. The main reasons for CaO capacity decay are pore blockage and sorbent sintering. The study of Alvarez et al. revealed that the pore blockage is negligible for the samples cycled at shorter carbonation times and sintering remains the main factor of capacity loss[13]. CaO has adsorption capacity of 0.785 g_{CO2}/g_{CaO}, while its closest competitor calcined dolomite (CaO.MgO) has the adsorption capacity of 0.46 $g_{CO2}/g_{sorbent}$. But as far as the multi cycle tests are concerned, dolomite has improved performance as compared to the CaO [14]. The carbonation of CaO is favourable in a temperature range of 600-750 °C under the atmospheric pressure. While, the regeneration of

the carbonated sorbent is a high temperature process and occurs at 850-1000 °C under the atmospheric pressure. Blamey et al. found that after multi-cycles the reactivity of the regenerated CaO particles reduces [15]. In previous studies [16-18], researchers concluded that addition of steam can enhance the carbonation reaction. The steam first reacts with available CaO and forms an intermediate product i.e. $Ca(OH)_2$. Later, this intermediate product undergoes carbonation reaction. The reaction mechanism is as follow;

$$CaO_{(s)} + H_2O_{(g)} \rightarrow Ca(OH)_{2(s)} \qquad \Delta H_{298K} = -109.18 \text{ kJ mol}_{CaO}^{-1} \qquad (1)$$

$$Ca(OH)_{2(s)} + CO_{2(g)} \leftrightarrow CaCO_{3(s)} + H_2O \qquad \Delta H_{298K} = -69.14 \text{ kJ mol}_{Ca(OH)2}^{-1} \qquad (2)$$

The main driving force for this adsorption of CO_2 on the active surface of the sorbent is the difference in the partial pressure of CO_2 between the surface of the sorbent and the equilibrium CO_2 partial pressure at that temperature[19].

In 2000, Lyonet al. proposed an interesting concept of H_2 production process. Lyon et al. and Kumar et al. defined 'unmixed steam reforming' (USR) and applied it specifically to apacked bed reactor configuration by using atlernative feed flows [20-22]**.** In this process fuel and air are not directly mixed but separately passed over the surface of the catalyst [23]. First, air is introduced on the surface of the catalyst, then it is discontinued, and fuel with steam is introduced after that either together or in sequence. The USR process uses oxygen transfer material (OTM), such as NiO, CuO, MnO etc., to provide heat for the endothermic SMR reaction. During the reduction of OTM, metal is regenerated and undergoes the cycle of reforming with the fuel gas and steam [12, 24]. The concept of unmixed combustion was studied in 1950 and this gives rise to the term chemical looping combustion (CLC) [25-27]. The terminology originally applied to the pilot plant reactor configurations with moving bed reactors. The CLC makes way for a new process referred to as the chemical looping

reforming (CLR) process. The CLR process too works on the same chemical principle as that of USR.

The CLR process operates in alternative cycles between 'steam reforming' and 'regeneration of the catalyst particles'. The heat generated during the oxidation of metal oxide is utilized in the endothermic SMR reaction (**eq. 3**). In the fuel reactor (FR), reforming and reduction reactions take place (**eq. 3-5**) while in the air reactor (AR) the regeneration of the catalyst takes place via oxidation reactions (**eq. 6**). In fixed bed, reactors are alternately used in 'FR' or 'AR' mode as the feeds are switched from reducing conditions to oxidising conditions, whereas for moving beds, FR and AR reactors house the same reactions (reduction + reforming, and oxidation, respectively) whilst the reactor solids are circulated between the two.

Iron, nickel, copper and manganese are the most promising OTM. The characteristics of all these metal oxides (Fe_2O_3, NiO, CuO and Mn_2O_3) were investigated in literature on the basis of their reactivity, regeneration ability and their ability to avoid carbon deposition. NiO was found the best amongst all these and it shows high selectivity towards hydrogen production. NiO does not agglomerate after many cycles of oxidation and reduction. Mn_2O_3 shows some minor signs of agglomeration, CuO does not show any structural change at 800°C but Fe_2O_3 shows a complete change of its structure at 900°C. So the reactivity was in the order of NiO/SiO_2>CuO/SiO_2> Mn_2O_3/SiO_2> Fe_2O_3/SiO_2[28]**.** Ni is the most interesting amongst all of the available OTM for reforming because of its strong catalytic properties [29]. The reaction scheme proposed by Kumar et al. in the fuel and the air reactor is given as[30]:

Fuel Reactor;

$$CH_{4(g)} + H_2O_{(g)} \leftrightarrow CO_{(g)} + 3H_{2(g)} \qquad \Delta H_{298K} = 206\ \text{kJ mol}_{CH4}^{-1} \qquad (3)$$

$$CO_{(g)} + H_2O_{(g)} \leftrightarrow CO_{2(g)} + H_{2(g)} \qquad \Delta H_{298K} = -41\ \text{kJ mol}_{CO}^{-1} \qquad (4)$$

$$NiO_{(s)} + \frac{1}{4}CH_{4(g)} \rightarrow \frac{1}{4}CO_{2(s)} + \frac{1}{2}H_2O_{(g)} + Ni_{(s)} \qquad \Delta H_{298K} = 43.7\ \text{kJ mol}_{NiO}^{-1} \tag{5}$$

Air Reactor;

$$Ni_{(s)} + \frac{1}{2}O_{2(g)} \rightarrow NiO_{(s)} \qquad \Delta H_{298K} = -244\ \text{kJ mol}_{Ni}^{-1} \tag{6}$$

Later on, Lyonet al. proposed another interesting approach by combining the CLR and SE-SMR process[21]. This concept was later named as the sorption enhanced chemical looping steam reforming (SE-CLSR) process. In this process, the carbonation reaction (**eq. 7**),

$$CaO_{(s)} + CO_{2(g)} \leftrightarrow CaCO_{3(s)} \Delta H_{298K} = -178.8\ \text{kJ mol}_{CaO}^{-1} \tag{7}$$

in the FRis used to enhance the performance of the reforming reaction, and the heat of catalyst oxidation is used for the regeneration of the sorbent [21, 31]. Rydén et al.**[32]**used three interconnected fluidized bed reactors having NiO as OTM and CaO as CO_2 acceptor. Rydén et al. developed a process model of SE-CLR process on Aspen plus. They studied the effect of sorption enhancement (SE) only on the WGS. Pimenidou et al. [17] proposed the packed bed reactor system for H_2 production from waste cooking oil. In the experimental work, reactor system contained NiO (18 wt.% NiO supported on Al_2O_3 from Johnson Matthey)as OTM and CaO as sorbent. Kulkarni et al.[33] proposed the gasification technology for the production of H_2 and sequestration ready CO_2. The efficiency of the process was better than the integrated gasification combined cycle (IGCC) process with conventional CO_2 separation.

The mathematical modelling of the SE-CLSR process in a packed bed is not reported in the literature. To fill this gap, a one-dimensional mathematical model of the SE-CLSR process is developed and implemented in gPROMS model builder 4.1.0® for the solution of model equations in this work. The overall model is divided into sub-models of the FR and AR, representing the reactor operating under fuel and steam feed, and the reactor operating under

air or O_2-enriched air stream, respectively. This may apply to a single reactor with alternating feed streams, or to several reactors operated with staggered feeds, similar to PSA reactors or regenerative heat exchangers. The modelling of reduction, SE-SMR and oxidation mechanisms is discussed first, followed by the overall modelling of the SE-CLSR process. The sub-models (oxidation/SE-SMR/reductions) are also validated against the experimental data reported in the literature [34-36]. The schematic of SE-CLSR process is shown in **Figure 1.**

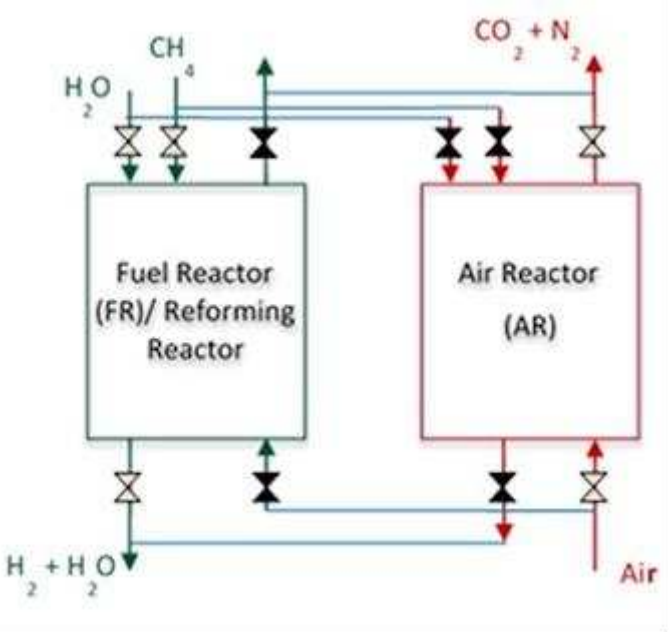

Figure 1: The schematic of SE-CLSR process in packed bed. ▶◀ = closed &▷◁ = open valves. Green reactor shown to operate in FR mode, red reactor in AR mode. When green reactor has cooled down, valves switch so that the green and red reactors operate in AR and FR mode respectively, completing chemical loop.

Before starting the modelling work, equilibrium results for SE-CLSR under various operating conditions of temperature, pressure, steam to carbon ratio (S/C), CaO/C and NiO/C are generated using chemical equilibrium with application (CEA) software. The thermodynamic

results for SMR, SE-SMR and SE-CLSR processes are compared in terms of CH_4 conversion, H_2 yield, H_2 purity and CO_2 capturing efficiency.

2. Thermodynamic analysis of SE-CLSR

Prior to the modelling of the SE-CLSR process, sensitivity analysis under equilibrium conditions is carried out to find out the optimum conditions for the SE-CLSR process. Antzara et al. [37] performed the thermodynamic equilibrium analysis using Aspen Plus and compared SMR, SE-SMR and SE-CLSR processes. They used the circulation beds in their process modelling work. The pressure range they used for the analysis was 1-25 bar, while in the industrial processes for H_2 production the pressure range used is 20-35 bar. In the present work, CEA is first used to generate the equilibrium results.

2.1 Methodology of equilibrium runs using CEA

The CEA software was used to generate the equilibrium data [44, 45]. This software is based on minimization of Gibbs free energy (G) [46]. The thermodynamic analysis was done by considering the gas species involved in the reactant and product streams are CH_4, H_2, CO, CO_2, H_2O, N_2, O_2, Ni, NiO, CaO and $CaCO_3$ using the option 'ONLY' in CEA, which allows to specify a restricted pool of species as potential equilibrium products The calculations of individual equilibrium molar outputs were performed on the basis of N_2 balance, which allowed to determine the total moles of product at equilibrium in post processing, and its product with the relevant mole fractions predicted by the CEA output. To study the effect of temperature, pressure and molar steam to carbon ratio of feeds (S/C) were fixed and the CEA code run in 'tp' mode, corresponding to an isothermal and isobaric process. Similarly, to study the pressure effect; temperature and S/C conditions were fixed, still in 'tp' mode.

The effects of molar ratios in the feed CaO/C and NiO/C on CH_4 conversion, H_2 purity, H_2 yield and CO_2 capturing efficiency are also studied under the equilibrium conditions, in addition to aforementioned temperature, pressure and S/C. To calculate the conversion of CH_4, the purity of H_2, H_2 yield (wt. % of CH_4) and CO_2 capturing efficiency following equations are used, where 'n' represents relevant molar amounts;

$$\mathrm{CH_4\ Conversion\ [\%]} = \frac{\left(n_{CH4,in} - n_{CH4,out}\right)}{n_{CH4,in}} \times 100 \quad (8)$$

$$\mathrm{H_2\ Purity\ [\%]} = \frac{n_{H2,out}}{\left(n_{H2,out} + n_{CH4,out} + n_{CO,out} + n_{CO2,out}\right)} \times 100 \quad (9)$$

$$\mathrm{H_2\ Yield\ [wt.\%\ of\ CH_4]} = \frac{(\mathrm{mol.\ weight\ of\ H_2} \times n_{H2,out})}{(\mathrm{mol.\ weight\ of\ CH_4} \times n_{CH4,in})} \times 100 \quad (10)$$

$$\mathrm{CO_2\ Capture\ [\%]} = \frac{\left(n_{CH4,in} - n_{CH4,out} - n_{CO,out} - n_{CO2,out}\right)}{n_{CH4,in}} \times 100 \quad (11)$$

2.2 Outputs of chemical equilibrium in SMR, SE-SMR and SE-CLSR

Although low pressure favours both SMR and SE-SMR, to investigate the SE-CLSR process with respect to its application in industrial process, elevated pressure (20-30 bar) conditions are used. In **Figure 2 (a-d)** effect of pressure on CH_4 conversion, H_2 purity, H_2 yield (wt. % of CH_4) and CO_2 capturing efficiency is shown. The effect of pressure is studied in the pressure range of 1-30 bar. As predicted, higher pressure results in lower conversion of CH_4 but still higher than the conversion achieved in case of SMR and SE-SMR processes under the same operating conditions. The drop in CH_4 conversion in SE-CLSR process is from 98.4% to 79.5% as the pressure increases from 1-30 bar. In the range of 20-30 bar, the drop in CH_4 conversion is 85.0% to 79.5%. The effect of pressure on H_2 purity is shown in **Figure 2 (b)**. It is clear that H_2 purity increases as pressure increases from 1-5 bar. The increase in H_2 purity is 95.5% to 97.2% as pressure increases from 1-5 bar. As pressure increases beyond 5

bar, the drop in H_2 purity is observed. H_2 purity goes down to 92.7% at 30 bar. Under the same conditions, drop in H_2 purity for SMR and SE-SMR is 76.4-56.5% and 94.4-90.8% respectively. So the purity of H_2 is higher in case of SE-CLSR process as compared to SMR and SE-SMR processes. In **Figure 2 (c)**, the yield of H_2 is lower in case of SE-CLSR as compared to SE-SMR process. The reduction of NiO in SE-CLSR process yields more carbon containing products (CO and CO_2) than H_2, hence lower yield of H_2 is achieved. On the other hand, reduction process is not considered in SE-SMR process. Hence, higher yield of H_2 as compared to SE-CLSR process is observed. In **Figure 2 (d)**, CO_2 capturing efficiency results show that higher pressure causes drop in CO_2 capturing efficiency. In case of SE-CLSR, the drop in CO_2 capturing efficiency is from 84.1% to 79.1% as pressure moves from 1-30 bar. It can be seen that there is increase in CO_2 capturing efficiency as pressure

moves from 1-10 bar, as in this range the partial pressure of CO_2 is higher than the equilibrium partial pressure, hence the carbonation reaction shifts towards product side [7].

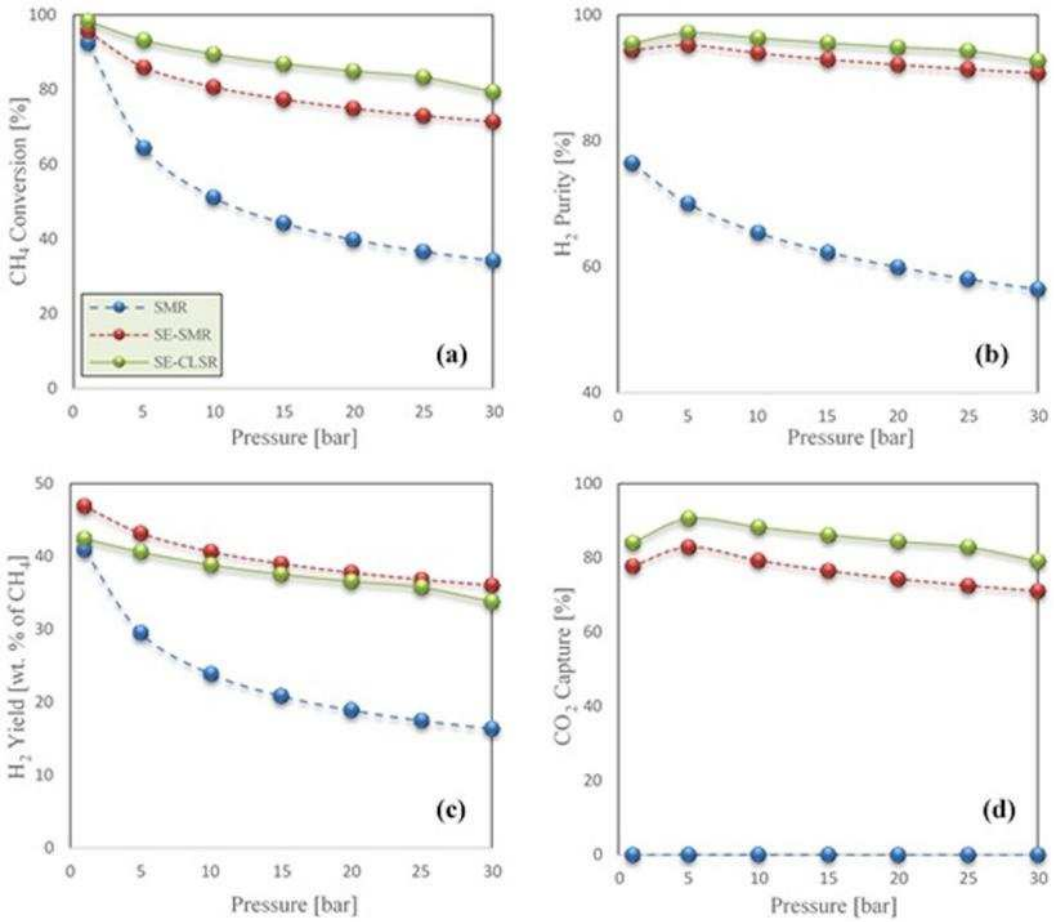

Figure 2: The effect of pressure on a) CH_4 conversion; b) H_2 purity; c) H_2 yield (wt. % of CH_4) and d) CO_2 capturing efficiency at 923 K, S/C of 3.0, CaO/C of 1.0 and NiO/C of 0.5

To study the effect of temperature on CH_4 conversion, H_2 purity, H_2 yield (wt. % of CH_4) and CO_2 capturing efficiency for SMR, SE-SMR and SE-CLSR processes, high pressure (30 bar) condition is used with a S/C of 3.0, a CaO/C of 1.0 and a NiO/C of 0.5. The increase in CH_4 conversion is from 22.4% to 86.1% as temperature varies from 300°C to 800°C in the SE-CLSR process. CH_4 conversion in SE-CLSR is higher than SMR and SE-SMR. H_2 purity and CO_2 capturing efficiency follow the same trend. In **Figure 3 (b)**, the maximum H_2 purities achieved at 973K are 93.9% and 91.0% in SE-CLSR and SE-SMR process respectively. The temperature of the system above 973K causes a drop in H_2 purity as the carbonation reaction

(**eq. 7**)deactivates at such a high temperature in favour of calcination, hence the drop in CO_2 capturing efficiency as observed in **Figure 3 (d)**.It is concluded that under 30 bar pressure, with S/C of 3.0, CaO: C of 1.0 and NiO:C of 0.5, 923-973K temperature range is the optimum range for the SE-CLSR process.

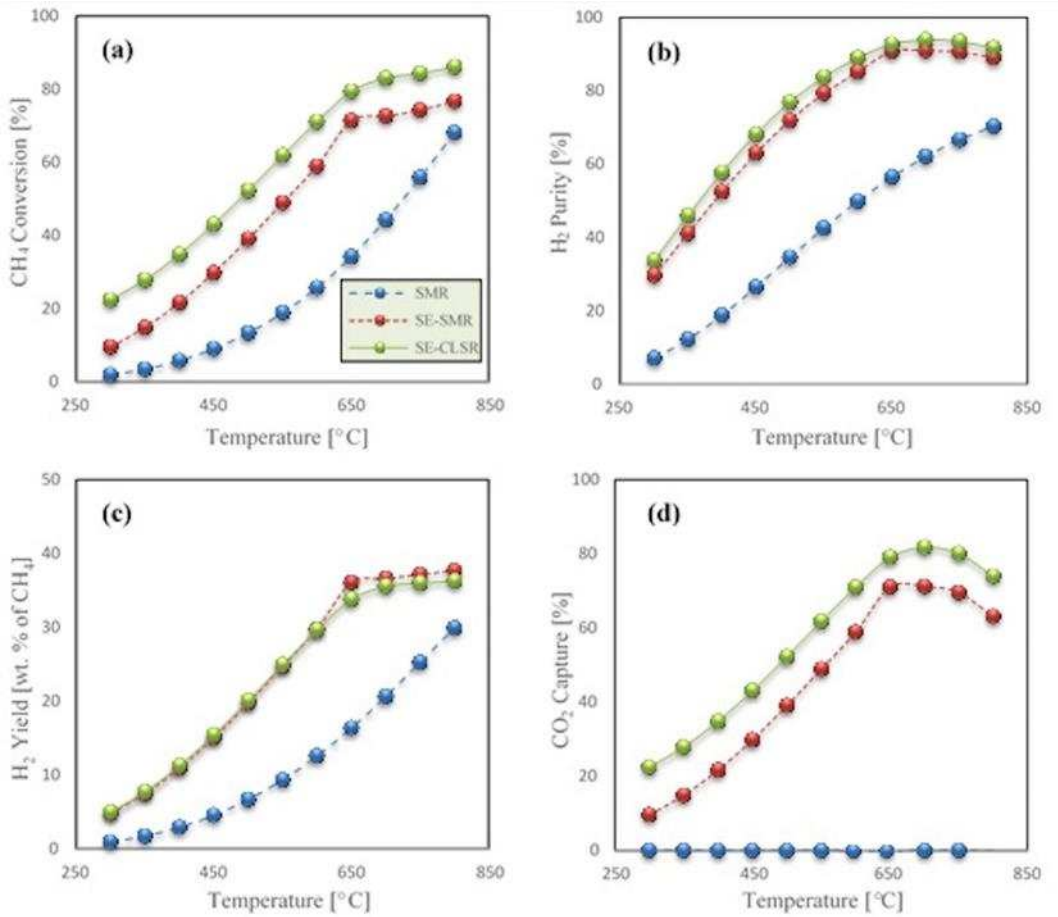

Figure 3: The effect of temperature on the a) CH_4 conversion; b) H_2 purity; c) H_2 yield (wt. % of CH_4) and d) CO_2 capturing efficiency at 30 bar, S/C of 3.0, CaO/C of 1.0 and NiO/C of 0.5

As in the reforming reactions, steam is required to convert the CH_4 into H_2 product. Excess of steam favours the reforming reaction towards more production of H_2. Although higher S/C (>2) favours CH_4 conversion and causes more formation of CO_2, this causes increase in the carbonation and hence promotes H_2 purity. But higher steam requirement has a negative

impact on the overall operational cost of the process, as energy is required to produce large quantity of steam. So there is always a trade-off between the selection of S/C and overall operational cost of the process. On an industrial scale, S/C of 3.0 is preferred for reforming reactions in order to minimise the possibility of coking. Under the equilibrium conditions the CH_4 conversion at S/C of 3.0 is 34.2%, 71.4% and 79.5% in SMR, SE-SMR and SE-CLSR process respectively at 923 K (650 °C) and 30 bar. Similarly the purity of H_2 at S/C of 3.0 is 56.5%, 90.8% and 92.7% in SMR, SE-SMR and SE-CLSR respectively at the same temperature and pressure.

The effect of the amount of CaO based sorbent on the performance of SE-CLSR process is shown in **Figure 4 (a-c)**. The maximum increase in CH_4 conversion is observed at CaO/C of 0.8 i.e. 80.5%. Further increase in the amount of CaO (> 0.8) has a negative effect on CO_2 capturing efficiency. Similarly, the purity and yield (wt. % of CH_4) of H_2 increase with increasing CaO/C as shown in **Figure 4 (b-c).** The purity of H_2 increases from 55.2% to 92.7% whereas the yield drops from 15.6% to 33.8% as CaO/C increases from 0-1. So the CaO/C between 0.8-1.0 is considered as the optimum ratio for SE-CLSR process under the conditions of 30 bar, 923 K and S/C of 3.0.

As the amount of NiO increases in the reactor, CH_4 conversion also increases as there is more demand in NiO reductant. But this makes less CH_4 available for reforming reactions hence lower yield of H_2 is achieved as shown in **Figure 5 (b)**. The yield (wt. % of CH_4) of H_2 drops from 36.1% to 31.7% as NiO/C increases from 0-1. The drop in H_2 yield is due to the consumption of H_2 or fuel-hydrogen during the reduction of NiO to Ni. Slight improvement in H_2 purity is observed as more conversion of CH_4 makes more H_2 and CO_2, so carbonation (eq. 7) shifts towards solid product. This results in H_2 with higher purity. The purity of H_2 increases from 90.8% to 95.2% as NiO/C increases from 0-1.0. This makes a trade-off between the yield of H_2 and CH_4 conversion [37]. Accordingly, a NiO/C of 0.5 could be

considered optimum as it still maintains a high H_2 yield (33.8 wt. % of CH_4) whilst CH_4 conversion, CO_2 capturing efficiency, and H_2 purity are 79.5%, 79.1%, 92.7% and respectively.

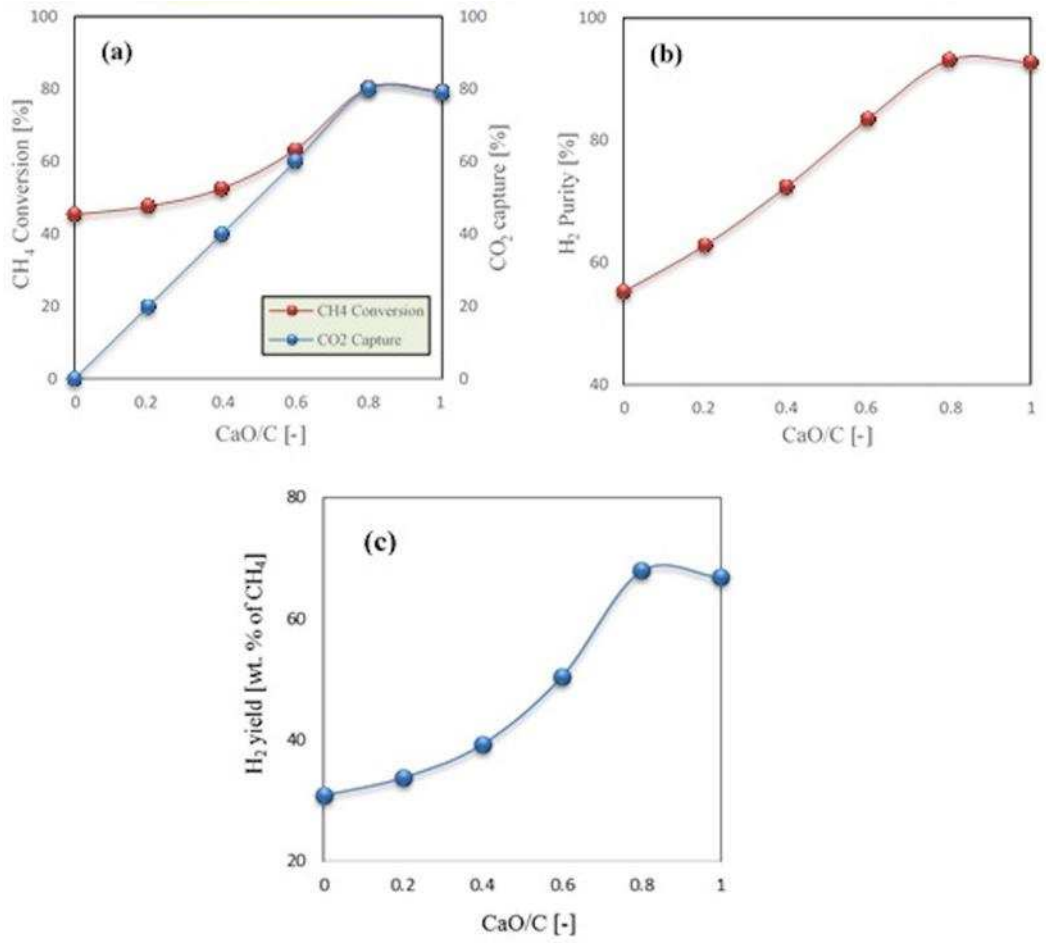

Figure 4: Effect of CaO/C on the a) CH_4 conversion; CO_2 capturing efficiency; b) H_2 purity; and c) H_2 yield (wt. % of CH_4); H_2 yield (wt. % of fuel available for H_2 producing reaction i.e. SR) at 30bar, 923K, S/C of 3.0 and NiO/C of 0.5

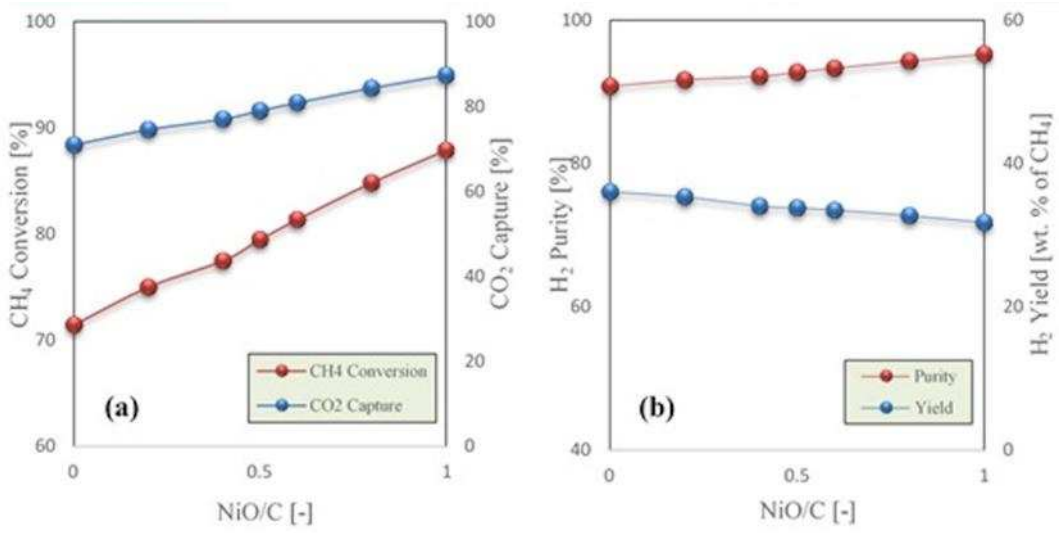

Figure 5: Effect of NiO/C on the a) CH_4 conversion; CO_2 capturing efficiency; b) H_2 purity; and H_2 yield (wt. % of CH_4) at 30bar, 923K, S/C of 3.0 and CaO/C of 1.0.

The above thermodynamic analysis is carried out by keeping in mind the industrial application of the SE-CLSR process. As already discussed, industrial H_2 production via SMR is a medium-high pressure process. Therefore, the optimum conditions for temperature, pressure, S/C, CaO/C and NiO/C obtained through thermodynamic analysis are 923-973 K, 30 bar, 3.0, 1.0 and 0.5 respectively.

3. Methodology of Mathematical Modelling of the dynamic process

A 1-D heterogeneous mathematical model of SE-CLSR in an adiabatic packed bed reactor is developed using gPROMS model builder 4.1.0®. This model accounts for mass and energy transfer in both gas and solid phase. In this model it is assumed that;

a) The flow pattern of gases in the packed bed reactor is plug flow in nature.

b) The temperature and concentration variations along the radial direction of the reactor are negligible.

c) The active surface of the catalyst and sorbent facilitates the reforming, reduction, sorption and oxidation reactions.

d) Ideal gas behaviour applies in this work.

e) There is no heat transfer from the system to the surrounding and from surrounding to the system. The operation is adiabatic in nature.

f) The size of the catalyst and sorbent are uniform and the porosity of the bed is constant.

3.1 Governing equations

One of the most important parameters in the design and the performance of the reactor is the kinetic mechanism. The overall behaviour of the reactor depends upon the set of reactions chosen to represent the chemical process, the values used for the pre-exponential factor and activation energy and the reaction rate equations used in modelling the reactor.

The reaction scheme and rate equations used in this work are summarized in **Table 1**. The oxidation of Ni based oxygen carrier (OC) [R_1]is very fast and highly exothermic in nature. The amount of heat released during oxidation mainly depends upon the concentration of O_2. The amount of carbon deposited on the surface of catalyst during chemical looping reduction cycle is oxidized to CO and CO_2 in the oxidation cycle [R_2-R_4]. The reduction reactions of Ni based OC [R_5-R_8] along with the SMR [R_9], WGS [R_{10}], overall reforming [R_{11}], dry reforming [R_{12}], methane decomposition [R_{13}], carbon gasification with steam [R_{14}], carbon gasification with CO_2 [R_{15}] and CO_2 adsorption [R_{16}] are the typical reactions included in the SE-CLSR process. The reactions between gas components and the catalyst support are neglected in this work due to the lack of data available in the literature [38].

Process	Reaction	Rate equation	Ref.
Oxidation of Ni	$O_{2(g)} + 2Ni_{(s)} \leftrightarrow 2NiO_{(g)}$ ΔH_r = -480,000 J mol_{O2}^{-1}	$R_1 = a_0 k_1 (1 - X_{Ni})^{2/3} C_{O_2} C'_{Ni}$	[39]
	$O_{2(g)} + C_{(s)} \leftrightarrow CO_{2(g)}$ ΔH_r = -393,500 J mol_{O2}^{-1}	$R_2 = a_0 k_2 (1 - X_C)^{1/2} C_{O_2} C'_C$	[40]
	$O_{2(g)} + 2C_{(s)} \leftrightarrow 2CO_{(g)}$ ΔH_r = -221,000 J mol_{O2}^{-1}	$R_3 = a_0 k_3 (1 - X_C)^{1/2} C_{O_2} C'_C$	[40]
	$O_{2(g)} + 2CO_{(g)} \leftrightarrow 2CO_{2(g)}$ ΔH_r = -566,000 J mol_{O2}^{-1}	$R_4 = \frac{k_4 C_{O_2} C_{CO}}{(1 + K_{CO,o} C_{CO})}$	[41]
Reduction of Oxygen carrier	$CH_{4(g)} + 2NiO_{(s)} \leftrightarrow 2Ni_{(s)} + 2H_{2(g)} + CO_{2(g)}$ ΔH_r = +161,400 J mol_{CH4}^{-1}	$R_5 = a_0 k_5 C_{CH_4} C_{NiO} C_{Ni} (1 - X_{NiO})$	[36, 42]
	$H_{2(g)} + NiO_{(s)} \leftrightarrow Ni_{(s)} + H_2O_{(g)}$ ΔH_r = -1,820 J mol_{H2}^{-1}	$R_6 = a_0 k_6 C_{H_2} C_{NiO} (1 - X_{NiO})$	[36, 42-45]
	$CO_{(g)} + NiO_{(s)} \leftrightarrow Ni_{(s)} + CO_{2(g)}$ ΔH_r = -153,500 J mol_{CO}^{-1}	$R_7 = a_0 k_7 C_{CO} C_{NiO} C_{Ni} (1 - X_{NiO})$	[36, 42, 45]
	$CH_{4(g)} + NiO_{(s)} \leftrightarrow Ni_{(s)} + 2H_{2(g)} + CO_{(g)}$ ΔH_r = +204,400 J mol_{CH4}^{-1}	$R_8 = a_0 k_8 C_{CH_4} C_{NiO} C_{Ni} (1 - X_{NiO})$	[36, 42, 46-48]
Steam methane reforming	$CH_{4(g)} + H_2O_{(g)} \leftrightarrow CO_{(g)} + 3H_{2(g)}$ ΔH_r = +206,200 J mol_{CH4}^{-1}	$R_9 = \frac{k_9}{p_{H_2}^{2.5}} \left(p_{CH_4} p_{H_2O} - \frac{p_{H_2}^3 p_{CO}}{K_I} \right) \left(\frac{1}{\Omega^2} \right)$	[42, 49, 50]
Water gas shift	$CO_{(g)} + H_2O_{(g)} \leftrightarrow CO_{2(g)} + H_{2(g)}$ ΔH_r = -41,200 J mol_{CO}^{-1}	$R_{10} = \frac{k_{10}}{p_{H_2}} \left(p_{CO} p_{H_2O} - \frac{p_{H_2} p_{CO_2}}{K_{III}} \right) \left(\frac{1}{\Omega^2} \right)$	[42, 49, 50]
Overall SMR	$CH_{4(g)} + 2H_2O_{(g)} \leftrightarrow CO_{2(g)} + 4H_{2(g)}$ ΔH_r = +165,010 J mol_{CH4}^{-1}	$R_{11} = \frac{k_{11}}{p_{H_2}^{3.5}} \left(p_{CH_4} p_{H_2O}^2 - \frac{p_{H_2}^4 p_{CO_2}}{K_{II}} \right) \left(\frac{1}{\Omega^2} \right)$	[44, 50, 51]

Dry methane reforming	$CH_{4(g)} + CO_{2(g)} \leftrightarrow 2CO_{(g)} + 2H_{2(g)}$ ΔH_r = +247,320 J mol_{CH4}^{-1}	$R_{12} = \frac{k_{12} p_{CH_4} p_{CO_2}}{1 + K_{CO_2} p_{CO_2}}$	[42, 44, 52]
Methane decomposition	$CH_{4(g)} + Ni_{(s)} \leftrightarrow C_{(s)} + 2H_{2(g)}$ ΔH_r = +74,820 J mol_{CH4}^{-1}	$R_{13} = \frac{k_{13} K_{CH_{4,d}} \left(p_{CH_4} - \frac{p_{H_2}^2}{K_{p,d}}\right)}{\left(1 + \frac{1}{K_{r,d}} p_{H_2}^{\frac{3}{2}} + K_{CH_{4,d}} p_{CH_4}\right)^2}$	[42, 44, 49, 52]
Carbon gasification with steam	$H_2O_{(g)} + C_{(s)} \leftrightarrow CO_{(g)} + H_{2(g)}$ ΔH_r = +131,320 J mol_C^{-1}	$R_{14} = \frac{\frac{k_{14}}{K_{H_2O,g}} \left(\frac{p_{H_2O}}{p_{H_2}} - \frac{p_{CO}}{K_{p,g}}\right)}{\left(1 + K_{CH_{4,g}} p_{CH_4} \frac{1}{K_{H_2O,g}} \frac{p_{H_2O}}{p_{H_2}} + \frac{1}{K_{r,g}} p_{H_2}^{\frac{3}{2}}\right)^2}$	[36, 42]
Carbon gasification with CO_2	$CO_{2(g)} + C_{(s)} \leftrightarrow 2CO_{(g)}$ ΔH_r = +172,500 J mol_C^{-1}	$R_{15} = \frac{\frac{k_{15}}{K_{CO_2,g} K_{CO,g}} \left(\frac{p_{CO_2}}{p_{CO}} - \frac{p_{CO_2}}{K_{p,g,CO_2}}\right)}{\left(1 + K_{CO,g} p_{CO} + \frac{1}{K_{CO_2,g} K_{CO,g}} \frac{p_{CO_2}}{p_{CO}}\right)^2}$	[42, 49]
CO_2 adsorption on $CaO_{(S)}$	$CaO_{(s)} + CO_{2(g)} \leftrightarrow CaCO_{3(s)}$ ΔH_r = -178,310 J mol_{CaO}^{-1}	$R_{16} = \frac{\eta}{M_{CaO}} \frac{dq_{CO2}}{dt}$	[35, 53, 54]

Table 1: Reaction scheme used for modelling the SE-CLSR process

The kinetic rate constants and the equilibrium constants used in the rate equations are temperature dependent terms and their equations as given in **APPENDIX A**. On the basis of the assumptions, reported above, the mathematical equations for mass and energy balance within the reactor filled with the sorbent and catalyst particles are listed in **Table 2**. The equations used to determine the physical properties, involved in the modelling, are given in

APPENDIX B.

Mass and energy balance in the gas phase ;
$\varepsilon_b\left(\frac{\partial C_i}{\partial t}\right)+\frac{\partial(uC_i)}{\partial z}+k_{g,i}a_v\left(C_i-C_{i,s}\right)=\varepsilon_b D_z\frac{\partial^2 C_i}{\partial z^2}$ $\varepsilon_b\rho_g C_{pg}\left(\frac{\partial T}{\partial t}\right)+u\rho_g C_{pg}\frac{\partial(T)}{\partial z}=h_f a_v(T_s-T)+\lambda_z^f\frac{\partial^2 T}{\partial z^2}$
Mass and energy balances in the solid phase;
$k_{g,i}a_v\left(C_i-C_{i,s}\right)=(1-\varepsilon_b)\rho_{cat}r_i+\upsilon\rho_{cat}r_i-(1-\upsilon)\,\rho_{ads}r_{ads}$ $\rho_{bed}C_{p,bed}\left(\frac{\partial T_s}{\partial t}\right)+h_f a_v(T_s-T)$ $=\upsilon(1-\varepsilon_b)\rho_{cat}\sum-\Delta H_{rxn,j}\,\eta_j R_j+(1-\upsilon)\,\rho_{ads}\sum-\Delta H_{ads}\,r_{ads}$
Mass balance for Nickel reduction;
$\left(\frac{dC_{Ni}}{dt}\right)=(2R_5+R_6+R_7+R_8)M_{Ni}\&\left(\frac{dC_{NiO}}{dt}\right)=-(2R_5+R_6+R_7+R_8)M_{NiO}$
Mass balance for carbon;
$\left(\frac{dC_C}{dt}\right)=R_j M_{Ni}C_C$

Table 2: Summary of mass and energy balance equations used to simulate 1-D heterogeneous packed bed reactor

On the basis of reactions involved, the rate of formation or consumption of 'i' component is given as;

$$r_i=\sum_{j=1}^{3}\eta_i\,\varphi_{ij}R_j \qquad i=CH_4, CO, CO_2, H_2 \text{ and } H_2O \qquad (10)$$

The boundary conditions and initial conditions used in solving the mass and energy balance equations are as follows;

Boundary conditions;

At reactor inlet (z = 0)

$C_i = C_{i,in}$; $T = T_{in}$; $T_s = T_{s,in}$; $P = P_{in}$

$C_{NiO} = C_{NiO,in}$; $C_{Ni} = C_{Ni,in}$

At reactor outlet (z = L)

$$\frac{\partial C_i}{\partial z} = 0 \quad ; \quad \frac{\partial T}{\partial z} = 0 \quad ; \quad \frac{\partial T_s}{\partial z} = 0$$

Initial conditions;

$C_i = C_{i,0}$; $T = T_o$; $T_s = T_{s,o}$; $X = 0$; $Carbon = 0$

$\& q_{CO2} = 0$

The values of boundary and initial conditions are presented in **APPENDIX C**.As an initial condition, it is considered that no gas component is present within the reactor so the concentration of gas species is zero at the start i.e. at t = 0. But by putting the concentration of H_2 to zero makes the rate of reforming reactions (R_9-R_{11}) infinite (denominator equals to zero). To avoid this, a very small initial concentration (~10^{-6}) of H_2 is used in the model.

In the reactor model linear and non-linear partial differential equations (PDEs), algebraic equations, and initial and boundary conditions are involved, and gPROMS was used to solve these equations. The sensitivity of the model was first checked for discretization ranging from 10-1000 intervals and model was found independent of the number of intervals. Finally, the reactor was axially discretized by 100 uniform intervals for this paper and output results were reported after every one second. The first order backward finite difference method (BFDM) was used to solve the PDEs using initial and boundary conditions as mentioned above. The model of the packed bed reactor was assumed to follow the non-ideal plug flow behaviour. In

gPROMS model builder 4.1.0 ® differential algebraic solver (DASOLV) was used to solve the ordinary differential equation (ODEs). DASOLV converts the PDEs into ODEs, and 4^{th} order Runge-Kutta technique was used to solve the system of equations.

4. Results and Discussion

The modelling results of SE-CLSR process are divided into two parts. In the first part individual models of reduction of NiO, SE-SMR oxidation of reduced Ni catalyst are validated. Later, the models of FR (reduction and SE-SMR model) and AR (oxidation model) are combined and cyclic process of SE-CLSR is studied.

4.1 Validation of NiO reduction under CH_4 feed

The experimental data of Iliuta et al. is used to validate the modelling of NiO reduction process [36]. They used a fixed bed micro-reactor apparatus to investigate the reduction and oxidation (redox) of the NiO catalysts having Al_2O_3 as support. The loading of the catalysts was 0.1g in powder form with particle diameter 140μm. They used CH_4 in Ar as the reducing gas for the OTM. Experiment was initiated with the supply of CH_4 to the reactor and Ar to the vent. After a period of 10 min, feeds were switched off and system was purged for 2 min before starting the oxidation cycle. The micro-reactor was of quartz material having 4mm internal diameter and 7.65 mm bed length. They conducted the reduction experiments in the temperature range 800-900 °C.

In **Figure 6 (a),** the outlet mole fractions of product gases are shown. The length of reduction period is 60 s. In the experimental work, the outlet composition of the product gases was delayed by 10-12 s, hence the results presented in figure 5 are adjusted accordingly. The delay in the output results is because of the residence time of the gases between the 3 way valve and the gas analyser. 10% CH_4 in Ar is used as the reducing gas in this process. The results show that within ~6 s the mole fraction of CH_4 decreases to 0.007 and 0.006 in both

model and experiment respectively. In this period CH_4 is entirely converted to CO, CO_2, H_2 and H_2O. The mole fraction of H_2O is highest at the start as compared to other product gases. This is because of reduction reactions (R_5 and R_6). As the OTM reduced to Ni and formation of H_2 takes place, this H_2 further reduced the NiO according to R_6 and H_2O is the dominant gas product at the start of the reduction process. The maximum mole fraction of H_2O obtained in the modelling and experimental work is 0.083 and 0.080 respectively.

During the initial stage of the reduction process, the formation of CO_2 is dominant as compared to the formation of CO. This confirms that CO_2 formation takes place according to R_5 and R_7 at the same time. The formation CO via R_8 causes increase in the amount of CO at the outlet of the reactor but at the same time this CO takes part in the reduction of NiO and formation of CO_2 is observed. So in the initial stage of the reduction process CO_2 amount is higher than the amount of CO. The mole fraction of H_2 is the highest in later part of the reduction process and it reaches 0.101 and 0.106 in model and experiment respectively. The rise in the amount of H_2 is steep in both model and experiment. As the amount of O_2 in OTM reduces, the formation of product gases also decreases and the amount of CH_4 at the outlet of the reactor increases.

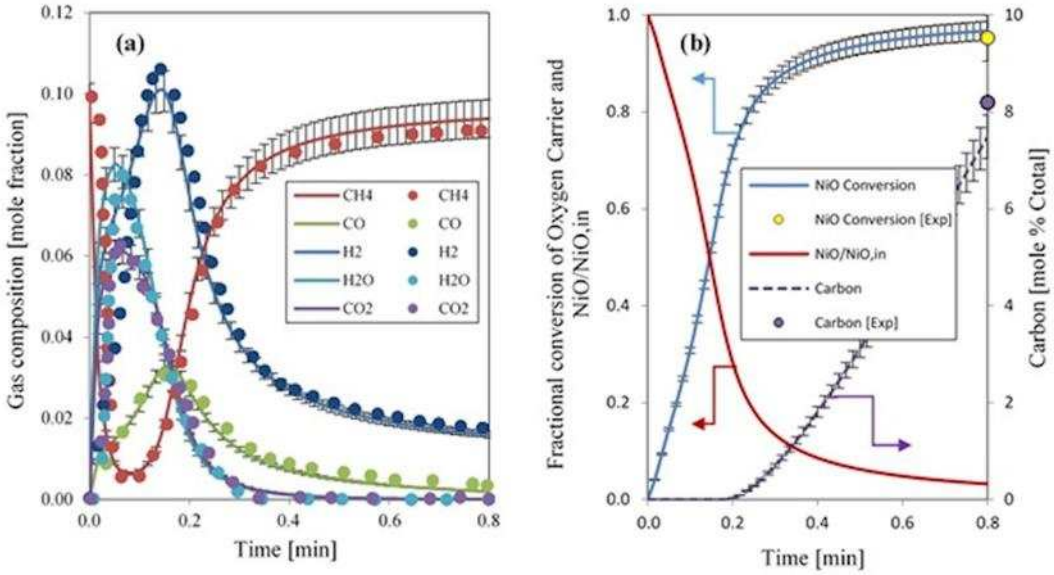

Figure 6: a) The distribution of gas products at the exit of reactor; b) The dynamic profile of NiO conversion and carbon formation under the operating conditions of 800 °C, 1bar and 10% CH_4 in Ar as reducing gas. Dots are the experimental values from [36] and solid lines are results generated in our modelling work.

Under the same operating conditions i.e. 800 °C, 1 bar and 10% CH_4 in Ar as reducing gas, the fractional conversion of NiO to Ni is reported as 0.96 in the experimental wok of Iliuta et al.In **Figure 6 (b)** the dynamic profile of NiO conversion is shown. It can be seen that the conversion of NiO reaches its maximum value very fast. After 60 s the conversion of NiO is 0.97 in the model, which is in excellent agreement with the experimental value of 0.96. In **Figure6 (b),** the dynamic profile of carbon formation on the surface of catalyst particle is also shown. The experimental value reported for carbon at the end of the reduction process is 8% carbon (mol% C_{total}). The modelling results are also in good agreement with experimental values. The formation of carbon is zero at the start as more O_2 is available for the formation of carbon containing product gases (CO and CO_2). As the amount of O_2 in OTM decreases, the formation of carbon on the catalysts surface increases. By analysing the formation of carbon, it is observed that when the conversion of NiO exceeds 72% the accumulation of

carbon on the surface of catalyst starts. The modelling and experimental results shown in **Figure 6 (a-b)** are in excellent agreement with each other and results are within 95% confidence interval.

4.2 Validation of SE-SMR process

The modelling results of SE-SMR are checked in terms of dry gas composition of product gases leaving the reactor. The modelling results of Fernandez et al. are used for our model validation [54]. Length of the reactor (L = 7 m), particle size (d_p = 0.01 m), bed porosity (ε_b = 0.5) and variables S/C (5.0), operating temperature (923 K), pressure (35 bar), mass flux of the gas phase (G_s = 3.5 kg m^2 s^{-1}) are adapted according to the values reported in the above mentioned literature. **Figure 7** shows the variation of gas compositions at the end of the reactor with time on stream.This figure is divided into pre-breakthrough period (t< 720 s), breakthrough (t = 720 to 1500s) and post breakthrough (t≥1500s). In the pre-breakthrough period, sorbent is active and most of the $CO_2$is adsorbed during SMR process.

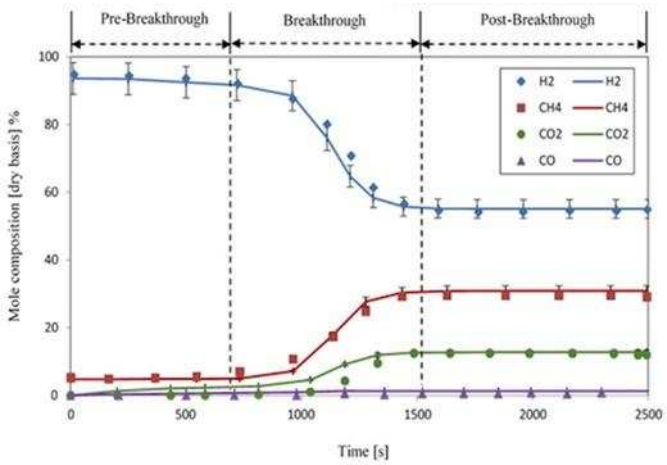

Figure 7: Product gases composition [dry basis] at the outlet of reactor at feed temperature of 923 K, S/C of 5.0, 35 bar and mass flux of the gas phase of 3.5 kg m^{-2} s^{-1}. Dots represented literature values [54] while solid lines are our modelling values

The adsorption of CO_2 from the product gases shifts the reforming reaction (**eq. 3**) in forward direction i.e. towards more production of H_2. In the pre-breakthrough period, H_2 mole percent is 94% and CO_2 mole percent is 0.1%, whilst unreacted CH_4 is 5.2%, indicating high conversion and high H_2 selectivity. In this section sorbent is at its maximum CO_2capturing efficiency. After 720 s, the amount of H_2 in the product gases diminishes and the amount of CO_2 increases. This is the start of breakthrough section. In this section, it is quite clear that CO_2 capturing efficiency of CaO based sorbent begins to wane. The sorbent is reaching saturation hence the amount of CO_2 in the product gases is increasing. Beyond 1500 s the saturated sorbent is no longer active and the only process happening within the packed bed reactor is conventional SMR process, with unconverted methane concentration rising to 33%. In the post-breakthrough period a steady state profiles for product gases composition is achieved.**Figure 7** shows an excellent agreement between the modelling values reported for SE-SMRby Fernandez et al.and the values generated in this work.

4.3 Validation of nickel oxidation under air and O_2 enriched air feed

To validate the mathematical model of the Ni oxidation, the experimental work of Monnerat et al. is used here [34]. A packed bed quartz reactor (ID = 9mm and L = 230mm) with Ni as catalyst (~210mg) was used. Temperature was monitored in the catalyst bed and pressure was measured upstream and downstream of it. The catalyst bed was heated from room temperature to 600 °C by using H_2 as feed gas. Later on H_2 was switched off and Ar was allowed to flush the system and temperature of the reactor was set to the desired temperature. The oxidation of catalyst was performed by supplying a controlled amount of air into the packed bed reactor [34, 55].

In this modelling work the oxidation process is assumed to be an adiabatic, so the temperature variation at the exit of the reactor with time is presented in **Figure 8 (a)**. The

modelling results are compared with the experimental variation of temperature under the conditions of 773K feed temperature, 1.5bar and 10%O_2 in Ar as feed gas for the oxidation process. An initial rapid rise in the temperature is observed and after 45s of operation the temperature decreases. This is because initially all Ni is available for oxidation process but as the conversion of Ni into NiO increases, the amount of O_2 in the exit also increases and temperature of the system goes down. The maximum predicted temperature achieved the modelling is 823K i.e. rise of 50K from the feed temperature. The temperature of the system goes to 776K after an operation of 180 s. It can be seen that modelling results are in excellent agreement with experimental values.

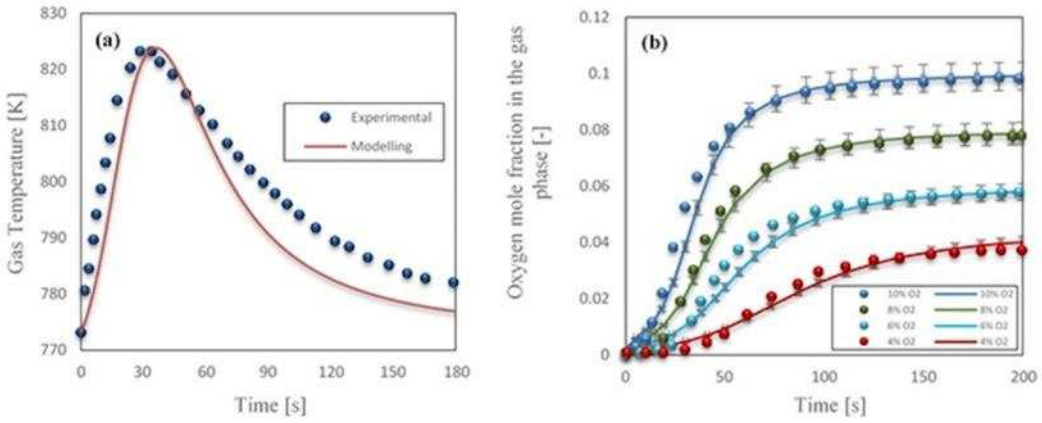

Figure 8: Ni oxidation model validation a) The dynamic temperature profile; b) Modelling and experimental response of outlet mole fraction of O_2 for different concentration of O_2 in feed gas under the operating conditions of 773 K feed temperature, 1.5 bar and 8% O_2 in feed gas. Dots are the experimental values [34, 55] and solid lines are the results generated in our modelling work

The model is further validated by varying the amount of O_2 in the feed gas. As in the oxidation process the vital parameter is the amount of O_2 in the feed, so the effect of O_2 concentration on the performance of the oxidation process is studied. In **Figure 8 (b)** experimental (dots) and modelling results (solid lines) of O_2 mole fractions at the exit of the

reactor for various concentration of O_2 in the feed are shown. The amount of O_2 in the feed has a positive effect on the rate of oxidation of Ni catalyst. The higher amount of O_2 in the feed (10%) causes the oxidation process to reach the maximum value earlier than the lower amount of O_2 (4%). The modelling results are in excellent agreement with the experimental results.

In previous sections, individual models of the FR and AR are developed and validatedagainst the modelling and experimental data reported in the literature separately.As discussed in the introduction, the overall SE-CLSR process in a packed bed reactor system is based on the cyclic process between FR and AR processes. At the start of the cycle CH_4, H_2O and N_2 are introduced in the packed bed reactor (FR), loaded with NiO and CaO particles. The feed is introduced ata fixed ratio of S/C and under the specific operating conditions of temperature and pressure. The reduction of NiO to Ni is followed by reforming reactions and adsorption of CO_2. After the complete reduction of the catalyst, the feed is switched to the mixture of O_2 in N_2. The reduced catalyst is re-oxidized and saturated sorbent is regenerated by the heat of oxidation reaction. After the complete oxidation of Ni to NiO and regeneration of sorbent, the next cycle of SE-CLSR starts by shifting the feed to CH_4, H_2O and N_2.

In the following section, the SE-CLSR process is studied under various operating conditions (temperature, pressure, S/C ratio). In this modelling of SE-CLSR process the Ni deactivation by the loss of Ni element is not considered, so the effect of temperature and pressure on the catalyst deactivation is neglected.

4.4 CASE STUDY 1: Cyclic study of SE-CLSR process

In this case study, 30 bar pressure is used to evaluate the performance of the SE-CLSR process during various cycles of FR and AR. The reactor configuration used in this section is the same as that used in section 4.2.

The SE-CLSR process starts with the FR. CH_4, H_2O and N_2 are used as feed in the FR cycle. The feed was introduced at 950 K (677 °C) and at S/C of 3.0. At the initial stage, CH_4 acts as a reducing gas and causes reduction of NiO to Ni. As reduction of NiO with CH_4 is highly endothermic process (R_5-R_8), so a drop in temperature of 50 K is observed at the start of the FR cycle as shown in **Figure 9**. The rise in the temperature from 900 K to 920.86K is observed after a run of ~400 s. This rise is mainly due to the heat released during the CO_2 adsorption reaction (R_{16}). As the standard heat of carbonation reaction is -178 kJ/mol, so a rise of ~20 K temperature is observed. This temperature (921 K) remains constant in the pre-breakthrough period (t < 550 s) and a sudden drop in the temperature is observed as the process crosses the pre-breakthrough period (t > 550 s). If the FR step is allowed to run after the breakthrough period, the steady state temperature reached in the post-breakthrough period (t >1200 s) will be ~882 K i.e. a drop of 68 K from the feed temperature. In the post-breakthrough period the sorbent is saturated, hence a sudden drop in temperature is observed. The feed gases are switched off after 550 s and at this stage the conversion of NiO to Ni is 99.97%. The red dot in **Figure 9** is the point where the FR cycle ends and the AR cycle begins. In this work, 21% O_2 in N_2 (air) is used as the feed for AR. The feed temperature of AR is the same as the feed temperature of FR (950 K). As in the FR, the conversion of NiO to Ni is not 100%, some NiO is present in the packed bed reactor at the start of the AR cycle. The overall oxidation of reduced Ni catalyst is a highly exothermic reaction and as the system is adiabatic, this causes the sudden rise of temperature within the packed bed reactor. The temperature during the AR cycle climbs to 1043 K (770 °C) in 450 s as shown in **Figure 9**. The rise in temperature is directly related to the amount of Ni left in the reactor for further oxidation. As the amount of Ni drops due to the conversion into NiO, the rate of oxidation reaction decreases and so does the temperature of the system. The conversion of Ni to NiO during this cycle is 89.8%. If more time was allowed for the AR step, a Ni conversion higher

than 99% could be achieved, but this would be at the expense of lower outlet temperature of the gases. So there is a trade-off between the temperature requirement at the outlet of AR and the conversion of Ni to NiO. The optimum temperature selected for AR is 1043 K and at this point the conversion of Ni is 89.8%. To achieve this temperature, the AR cycle is run for 450 s and after this the feed gases are again switched back to the feed gases for subsequent FR step. This completes one cycle of SE-CLSR process and at the end of this cycle 70% CH_4 conversion and 86.2% H_2 purity is obtained.

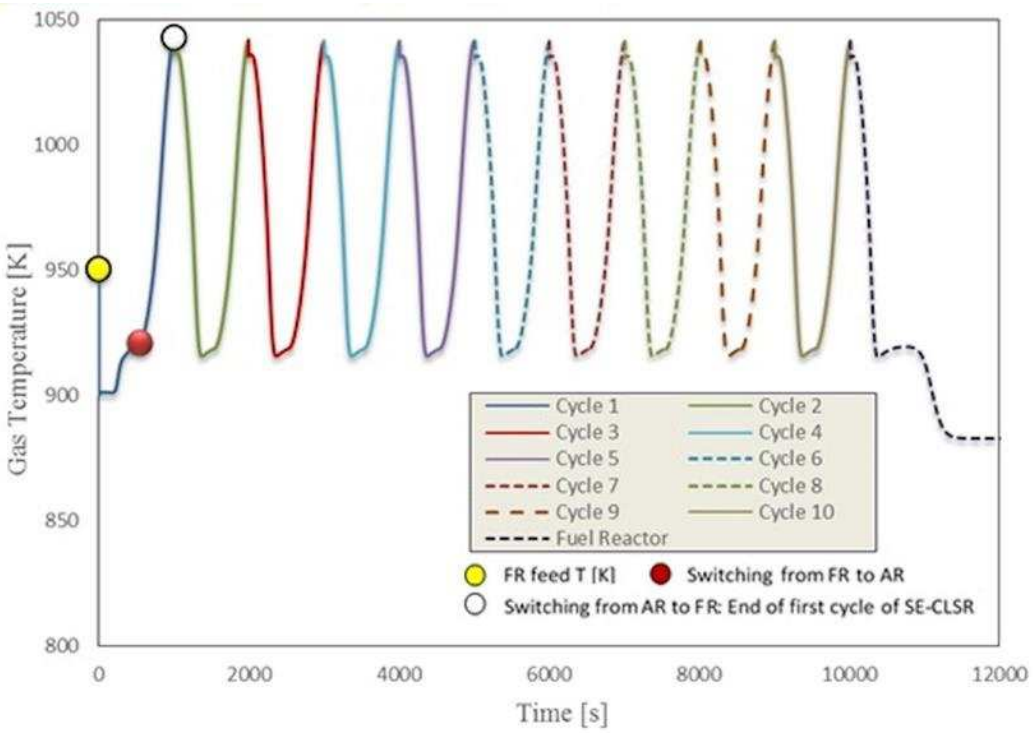

Figure 9: The dynamic profile of temperature in the packed bed reactor system of the SE-CLSR process. The SE-CLSR process is run for 10 complete cycles under the operating conditions of 950K, 30 bar, S/C of 3, CaO/C of 1, NiO/C of 0.5 and 21%O_2 in N_2 as feed for the AR.

This scheme of alternative cycles of FR and AR is allowed to run for 10 cycles. In 11th cycle, only modelling results of FR cycle are presented. It can be seen in figure 8 that if FR is allowed to run till the steady state is achieved, the temperature of the process drops to a minimum value of 882 K. In this period, only reforming reactions are dominating as sorbent is already saturated.

The dynamic profiles of dry mole fraction of product gases and gas temperature, in the second FR step (cycle 2), is shown in **Figure 10**. It can be seen that the amount of CH_4 is almost zero at the very start of the process (first 20 s) indicating 100% conversion of CH_4 during reduction reactions. As soon as the amount of NiO decreases, the conversion of CH_4 also drops. In the pre-breakthrough period, the mole % (dry basis) of CH_4 and CO_2 at the exit of the reactor are in steady state at 11.5% and 0.9% respectively. As soon as the process approaches the breakthrough period ($t < 550$ s), the FR system is switched to AR. The red dot in the figure is the switching point from FR to AR. At this point temperature of the system is 919 K (646 °C).

In the breakthrough period ($550 < t < 1200$ s) the drop in the concentration of H_2 is observed as the sorbent is reaching towards maximum saturation and less sorbent is available for CO_2 adsorption. In the post-breakthrough period ($t > 1200$), the gases concentration reach steady state. The steady state mole % (dry basis) of H_2 is 50.7%. Hence a drop in mole % of H_2 from 87.6% to 50.7% is observed in post-breakthrough period.

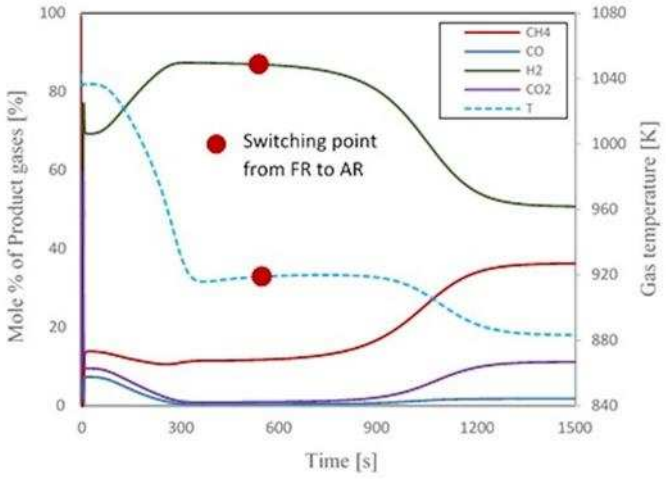

Figure 10: The dynamic profiles of mole% of product gases [dry basis] and gas temperature in the second cycle of FR under the operating conditions of 30bar, 950K feed temperature and S/C of 3.0

The variation for SMR, carbonation and reduction reaction rates along the length of the reactor during the first cycle of FR is shown in **Figure 11 (a)**. It shows that the reduction reactions have significant rate along the length of the reactor. The reduction of NiO to Ni produces CO_2, the sorbent captures the CO_2 and enhances the reduction reaction rate. So, the capturing of CO_2 at the start of the process promotes the reduction process and it can be seen in **Figure 11 (b)**. The dotted lines are the modelling results for the reduction rates in the absence of sorbent while the solid lines are for the reduction rates in the presence of sorbent. The enhancement of reduction rates in the presence of sorbent, promotes the fast conversion of NiO to Ni in the FR cycle. Later, along the length of the reactor as NiO is converted to Ni, both SMR and carbonation reactions start dominating the process.

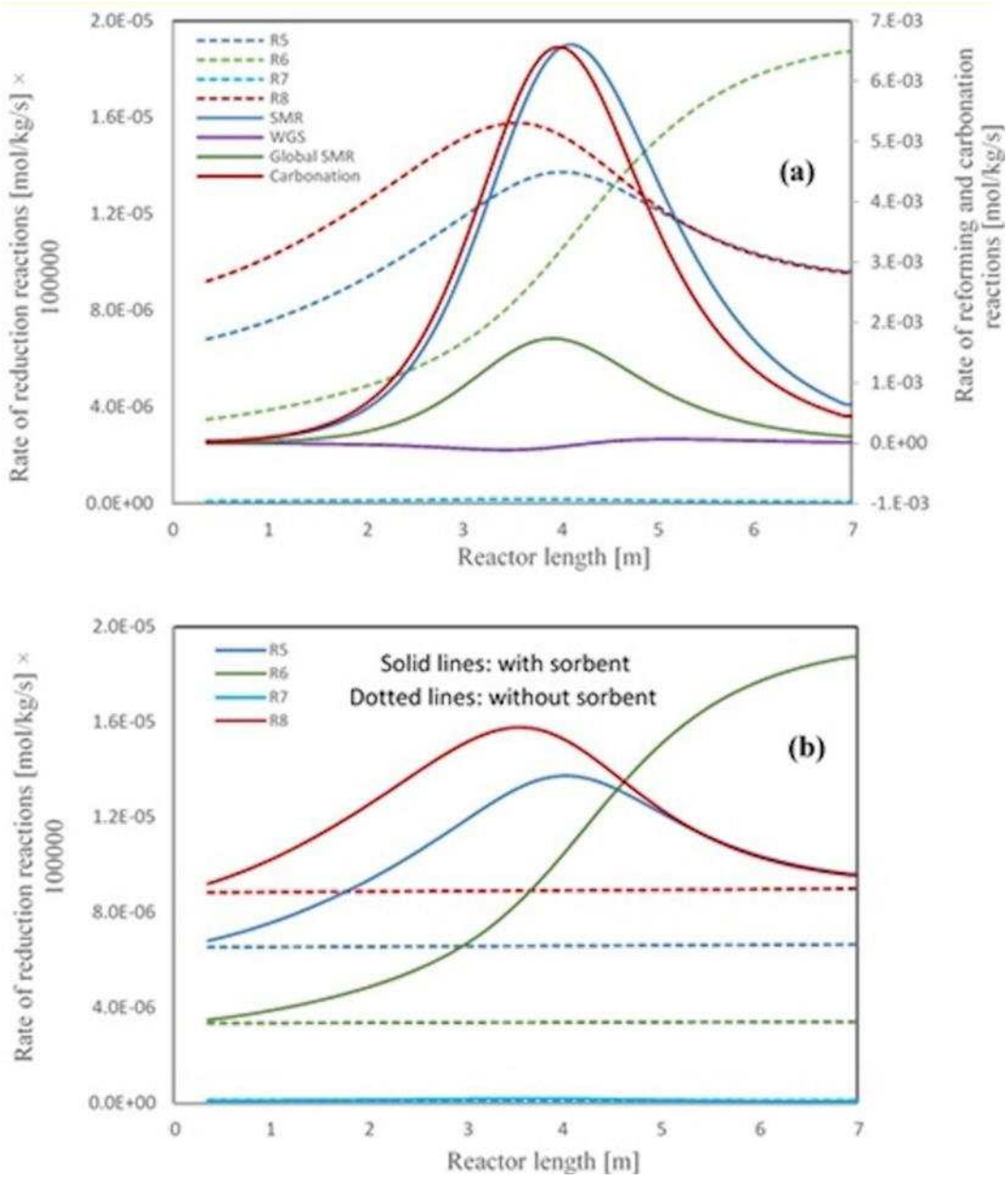

Figure 11: The profile of a) rate of reaction of SMR, carbonation and reduction reactions; b) rate of reduction reactions in the presence of sorbent and without sorbent along the length of reactor, in the first cycle of the FR, under the operating conditions of 30bar, 950K feed temperature and S/C of 3.0 (R5-R8 are the reduction reactions listed in table 1)

The variation in CH_4 conversion, H_2 purity, H_2 yield (wt. % of CH_4) and CO_2 capturing efficiency during 11 cycles of SE-CLSR is presented in **Figure 12**. The change in CH_4 is very negligible as it varies from 70.81% to 70.77% during 11 cycles of the SE-CLSR process. This shows that cyclic operation of the SE-CLSR process is very stable. The equilibrium value of CH_4 conversion under the same operating conditions is ~82%. The purity and yield (wt. % of CH_4) of H_2 are also not affected during 11 cycles of the SE-CLSR process. At the end of the 11^{th} cycle the purity of H_2 and H_2 yield (wt. %) is 86.9% and 28% against the equilibrium value of 93.9% and 35% respectively. The CO_2 capturing efficiency remains constant at 67.4%, compared to the equilibrium value of 81.8%. This is caused by the kinetics used for the carbonation reaction.

Although the values of CH_4 conversion, purity yield (wt. % of CH_4) of H_2under high pressure conditions are lower than equilibrium and significantly below 100%, keeping in mind the operational constraints of industrial process for H_2 production (scale of plant, throughput), we need to select the high pressure conditions over lower pressure. As the variation of output results with number of cycles is almost negligible, so in the next section the sensitivity of the SE-CLSR process is checked for temperature and S/C while considering only two cycles of the SE-CLSR process.

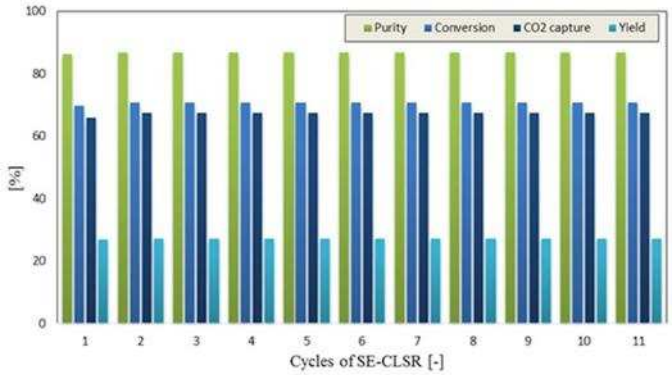

Figure 12: Comparison of CH_4 conversion, H_2 purity, H_2 yield (wt. % of CH_4) and CO_2 capturing efficiency achieved during 11 cycles of the SE-CLSR process under the operating conditions of 950 K, 30 bar and S/C of 3.0

4.5 CASE STUDY 2: Sensitivity analysis on temperature, S/C, Ni/C, Ca/C

In this section, the effect of temperature and S/C on the performance of SE-CLSR is first studied. The output of mathematical modelling will be compared with the equilibrium data generated using CEA. In **Figure 13 (a-b),** the effect of temperature on the output mole % (dry basis) of H_2 and CO_2 is shown. At 873 K temperature, the amount of CO_2 is almost zero (0.2 mole % on dry basis) in the pre-breakthrough period and the amount of H_2 is ~83 mole % on a dry basis. As the feed temperature increases from 873 K to 923 K, the amount of CO_2 in the exit gases also increases along with the amount of H_2. It can be seen in **Figure 13 (a-b)** that the amount of CO_2 is maximum at 1023 K temperature. This shows that the sorbent is not very active in this temperature range, hence the CO_2 capturing efficiency is not very high. The pre-breakthrough period is different for different temperature conditions. At 923 K and 973 K temperature the amount of H_2 in the pre-breakthrough period is 87.14% and 87.32% respectively and the amount of CO_2 is 0.36% and 0.96% respectively. At 1023 K, the concentration of H_2 (84.6 mole% on dry basis) is also lower than that at 973K temperature. The increase in the temperature of the SE-CLSR process promotes the CH_4 conversion as

shown in **Figure 14**. The conversion of CH_4at 873 K and 973 K is 62.4% and 71.7% respectively. The increase in H_2 yield (wt. %) is 23.8-27.7% as temperature increases from 873-973 K. The higher temperature shifts the reforming reaction in the forward direction and enhances the conversion of CH_4 but as the temperature increases from 973K to 1023K, a drop in CH_4 conversion is observed. The new value obtained at 1023K is 70.5%. Similarly the drop in CO_2 capturing efficiency is observed as temperature increases from 973K to 1023K (68.3-60.0%). This drop in CO_2 capturing efficiency has a direct adverse effect on the purity of H_2. The H_2 purity drops from 87.3% to 84.6% as temperature increases from 973K to 1023K. This confirms that the sorption reaction is not favourable as temperature increases beyond 973K. The kinetics used for the carbonation reactions are not favourable for such a high temperature conditions.

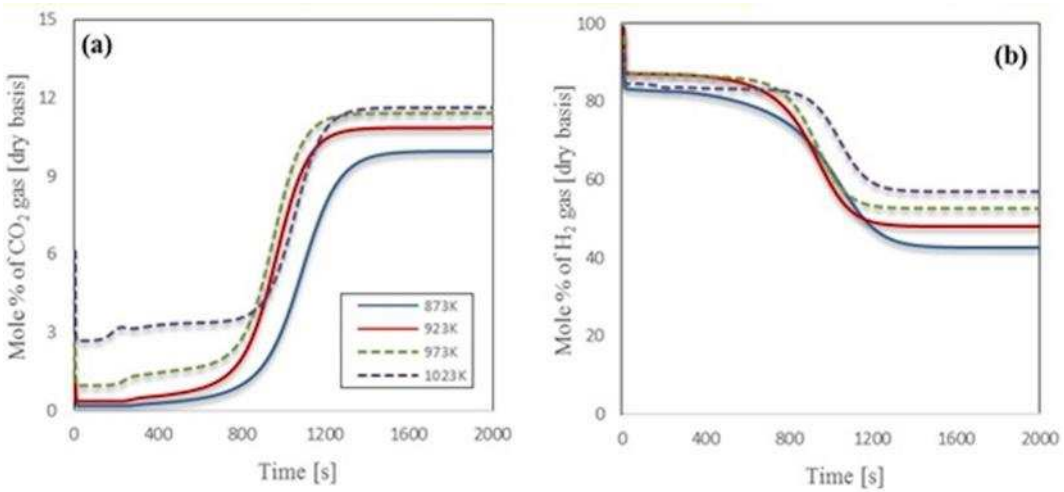

Figure 13: Effect of temperature on the outlet composition of a) H_2 and b) CO_2 at 30 bar and S/C of 3.0

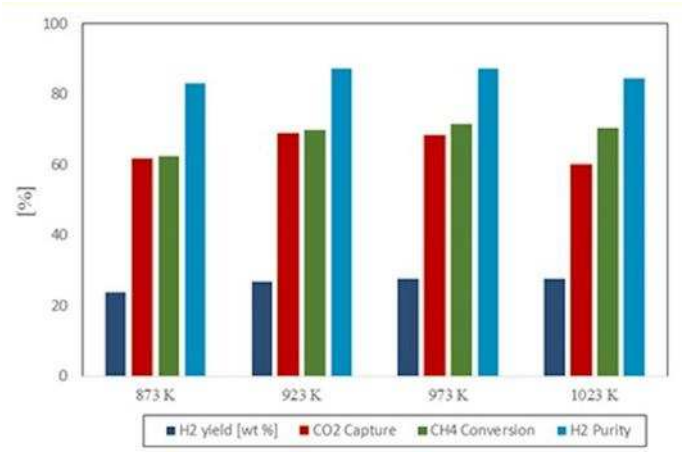

Figure 14: Effect of temperature on the H_2 yield (wt. % of CH_4), CH_4 conversion, CO_2 capturing efficiency and H_2 purity at 30 bar, S/C of 3.0

In **Figure 15,** the effect of S/C on CH_4 conversion, H_2 purity, H_2 yield (wt. %) and CO_2 capturing efficiency is shown. The optimum temperature and pressure conditions obtained from previous sections (973K and 30bar) are used. It can be seen from the graph that higher S/C favours more conversion of CH_4 to H_2 as more steam is available for the reforming reactions. The maximum conversion is achieved at the highest S/C considered (4.0) i.e. 81.9% and under the same operating conditions, the CO_2 capturing efficiency, the purity and yield (wt. % CH_4)of H_2 are 74.9%, 91.0% and 32% respectively. Although high S/C favours the SE-CLSR process, it puts a burden on the utility cost of the process as more energy is required to generate more steam for the process. So there is a trade-off between the operational cost and the selection of S/C. The optimum value picked is 3.0 as this value is also used in industrial processes of H_2 production to prevent carbon deposits.

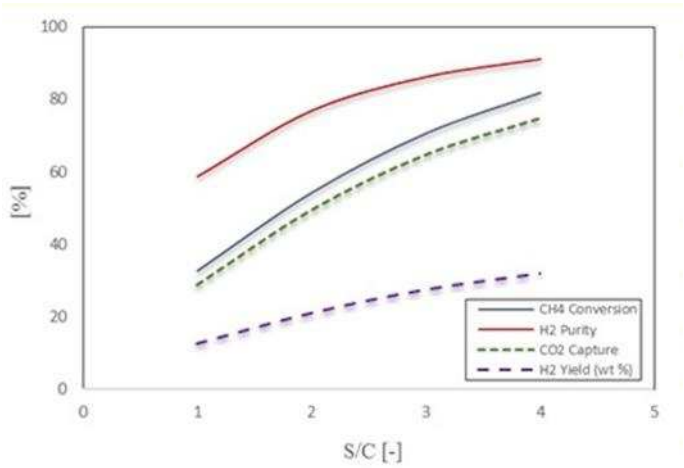

Figure 15: Effect of S/C on the CH_4 conversion, H_2 yield (wt. % of CH_4), H_2 purity and CO_2 capturing efficiency under the operating conditions of 973K, 30bar, CaO/C of 1.0 and NiO/C of 0.5.

The reduction reactions are endothermic in nature and cause drop in the temperature of the system. Later on, carbonation causes a sudden rise in the temperature because of its exothermicity. As long as the sorbent is not saturated, the temperature of the system remains higher than the feed temperature. The effect of S/C on the temperature of the SE-CLSR at the outlet of the reactor is shown in **Figure 16**. It can be seen that there is very negligible effect of S/C on the temperature profile of the packed bed reactor in SE-CLSR process with time. The maximum temperature is almost the same in all cases of S/C i.e. ~945K. If the FR is allowed to run for a considerable time so that steady state is reached then the minimum temperature reached in all cases is almost the same as well i.e. ~900K.Another important factor that can affect the performance of the SE-CLSR process is the mass flux of the gas phase (G_s). The higher G_s causes lesser time for the gases to spend within the reactor system. Hence,G_s is inversely proportional to the pseudo contact time. In **Figure 17,** the effect of G_s on the outlet composition (dry basis) of H_2 and CO_2 is presented. Higher G_s causes shorter pre-breakthrough period (onset of breakthrough occurs earlier). Conversely, lower G_s causes

longer pre-breakthrough. The pre-breakthrough period in case of mass flux of the gas phase of 2, 3.5 and 5 $kgm^{-2}s^{-1}$ is 1300s, 600s and 300s respectively. The values for CH_4 conversion, H_2 yield and H_2 purity for mass flux of the gas phase of 2, 3.5 and 5 $kgm^{-2}s^{-1}$ are shown in **Table 3**. It can be seen that these variations in gas mass velocities do not affect the CH_4 conversion, purity and yield (wt. % of CH_4) of H_2 but the time required to complete a cycle of SE-CLSR process. In the conventional SMR process, the equilibrium concentration of the product gases at the exit of the reactor reaches at the gas velocity of 1.5-2 m/s [56]. While the carbonation reaction is slower reaction as compare to SMR, hence longer residence time or slow gas velocity is required to reach the equilibrium concentration of the product gases at the outlet of the reactor. 3.5 $kgm^{-2}s^{-1}$mass flux (gas velocity equivalent to 0.448 m/s) is selected as the optimum value for the SE-CLSR process as it gives considerable time for the sorbent to react its full capacity without disturbing the cycle duration of the SE-CLSR process.

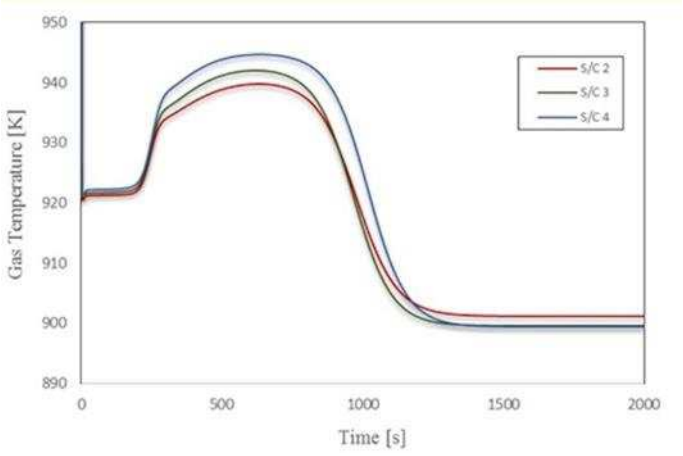

Figure 16: Effect of S/C on the temperature profile of the SE-CLSR process under the operating conditions of 973K, 30bar, CaO/C of 1.0 and NiO/C of 0.5.

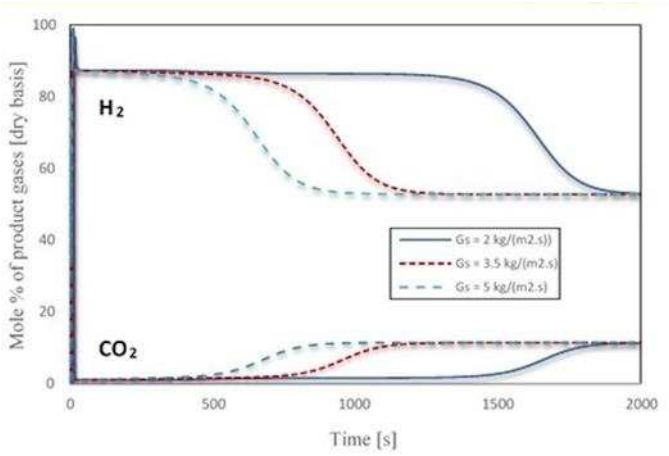

Figure 17: Effect of mass flux of the gas phase on the outlet composition of H_2 and CO_2 under the operating conditions of 973K, 30bar and S/C of 3.0

G_s [kg m^{-2} s^{-1}]	**CH_4 conversion [%]**	**H_2 yield [wt. % of CH_4]**	**H_2 purity [%]**
2	70.61	27.45	85.99
3.5	70.22	27.32	85.77
5	69.79	27.14	85.60

Table 3: Effect of mass flux of the gas phase on CH_4 conversion, yield (wt. % of CH_4) and purity of H_2 under the operating conditions of 973 K, 30 bar and S/C of 3.0

5. Conclusion

The adiabatic SE-CLSR process in a packed bed reactor using methane feedstock for H_2 production is simulated using 1-dimensional heterogeneous model of the process. The model equations are solved using the 1st order backward finite different method in gPROMS. The model of the SE-CLSR is run for 11 cycles under the adiabatic conditions. The FR cycle and the AR cycle are simulated and the results are validated against published experimental data. The packed bed reactor of SE-CLSR process is run under various operating conditions of temperature, pressure, S/C and mass flow velocities to study the sensitivity of the process. The effect of these operating parameters is studied under the equilibrium conditions and later on compared with the dynamic model outputs. It is concluded from the results that there is a negligible effect observed on CH_4 conversion, H_2 purity, H_2 yield (wt. % of CH_4) and CO_2 capturing efficiency during the various number of the SE-CLSR cycles. The effect of pressure is positive on the performance of SE-CLSR process, but as the pressure exceeds 5 bar, the conversion and CO_2 capturing efficiency decreases. While keeping in mind the H2 production on industrial scale, the pressure of 30 bar is used to generate data at different operating temperatures (873-973 K). At 873 K, 62% CH_4 conversion and 83% H_2 purity are achieved. As the temperature increases to 973 K, the CH_4 conversion and H_2 purity both increase to 72% and 87% respectively. The temperature higher than 973 K reduces both H_2 purity and CO_2 capturing efficiency as the carbonation reaction is not active at such a higher temperature. So 973 K is selected as the optimum temperature for the SE-CLSR process operated under 30 bar pressure. The S/C of 3.0 gives the optimum value for CH_4 conversion and H_2 purity as the higher values of S/C are not favourable as far as the operational cost of the process is concerned. The higher S/C increases steam requirement and hence more operational cost. So, despite of its positive effect on CH_4 conversion and H_2 production, S/C

higher than 3 is not recommended for the industrial scale production of H_2. It is concluded that the gas mass velocity has no effect on the production of H_2 but the higher mass flux of the gas phase reduces the pre-breakthrough period and the cycle duration. The mass flux of the gas phase of 3.5 kg $m^{-2}s^{-1}$ is selected as the optimum value for 30 bar and S/C of 3. The sensitivity analysis demonstrates that the developed model of the SE-CLSR process gives significantly higher purity of H_2 and CH_4 conversion under high pressure (30 bar) conditions as compared to the conventional SMR process. This model can be applied to simulate continuous production of H_2 using either two or multiple packed bed reactors. In future, this model will be used to simulate the production of H_2 in ammonia plant.

6. Acknowledgement

The following are gratefully acknowledged: The financial support of University of Engineering and technology (UET) Lahore, Pakistan, Dr. Feng Cheng for help with CEA modelling and Prof. Mojtaba Gadhiri, University of Leeds, for access to the license for gPROMS model builder 4.1.0®.We are also thankful for UKCCSRC EPSRC consortium (EP/K000446/1) call 2 grant 'Novel Materials and Reforming Process Route for the Production of Ready-Separated $CO_2/N_2/H_2$ from Natural Gas Feedstocks'.

NOMENCLATURE	
a_o	initial specific surface area of the oxygen carrier[$m^2 kg_{carrier}$]
C_C	Carbon concentration [$kg_C\ kg_{carrier}^{-1}$]
C_i	Concentration of gases i [mol m^{-3}]
$C_{i,o}$	Initial concentration of gases i in gas phase [mol m^{-3}]
$C_{i,s}$	Concentration of gases i in solid phase [mol m^{-3}]
C_{Ni}	Ni concentration [$kg_{Ni}\ kg_{carrier}^{-1}$]
C_{NiO}	NiO concentration [$kg_{NiO}\ kg_{carrier}^{-1}$]
$C_{p,bed}$	Heat capacity of catalyst bed [J kg^{-1} K^{-1}]
C_{pg}	Heat capacity of gases [J kg^{-1} K^{-1}]
$C_{s,o}$	Initial concentration of gases i in solid phase [mol m^{-3}]
C_{total}	Total amount of carbon
D_i	Effective diffusion coefficient [m^2 s^{-1}]
D_m	Average molecular diffusivity [m^2 s^{-1}]
D_z	Axial dispersion coefficient [m^2 s^{-1}]
d_p	Particle diameter [m]
E_j	Activation energy of reaction j [J mol^{-1}]

G	Gibbs free energy [J]
G_s	Gas mass flow velocity [kg m^{-2} s^{-1}]
ΔH_i	Heat of adsorption of i specie [J mol^{-1}]
$H_{rxn,j}$	Heat of reaction of j reaction [J mol^{-1}]
h_f	Gas to solid heat transfer coefficient [W m^{-2} s^{-1})]
j_D, j_H	Chilton-Colburn factor for mass and heat transfer
$k_{g,i}$	Gas to solid mass transfer coefficient of component i [m^3 m^{-2} s^{-1})]
k_j	Kinetic rate constant of reaction j
k_{oj}	Reference temperature dependent kinetic rate constant of reaction j
K_j	Thermodynamic equilibrium constant
K_i	Adsorption constant of species i
K_{oi}	Reference adsorption constant of species i
K_D	Viscous loss term in pressure drop calculations [Pa s m^{-2}]
K_v	Kinetic loss term in pressure drop calculations [Pa s^2 m^{-3}]
P_i	Partial pressure of species i [bar]
P	Total gas pressure [bar]
P_o	Initial pressure of the system [bar]
Pr	Prandtl number
r_{ads}	Rate of adsorption of CO_2 [mol kg^{-1} s^{-1})
r_i	Rate of formation or consumption of species i [mol kg_{cat}^{-1} s^{-1}]

R_j	Rate of reaction j [mol kg_{cat}^{-1} s^{-1}]
R_g	Ideal gas constant [J mol^{-1} K^{-1}]
Re	Reynolds number
s	Active site of the catalyst
Sc_i	Schmitt number
T	Gas temperature [K]
T_o	Gas inlet temperature [K]
T_s	Catalyst temperature [K]
$T_{s,o}$	Initial catalyst temperature [K]
u	Velocity of the gases [m s^{-1}]
X_C	Carbon conversion
X_{NiO}	NiO conversion
z	Axial dimension [m]
GREEK LETTERS	
Ω	Unit less term used in reaction kinetics
ε_b	Bed porosity
η_j	Effectiveness factor of reaction j
λ_g	Average gas thermal conductivity [W m^{-1} K^{-1}]
λ_s	solid thermal conductivity [W m^{-1} K^{-1}]
λ_z^f	Effective thermal conductivity [W m^{-1} K^{-1}]

μ_g	Average gas viscosity [kg m^{-1} s^{-1}]
μ_i	Chemical potential of component i [J mol^{-1}]
ρ_{ad}	Adsorbent density [kg m^{-3}]
ρ_{bed}	Bed density [kg m^{-3}]
ρ_{cat}	Catalyst density [kg m^{-3}]
ρ_g	Gas density [kg m^{-3}]

APPENDIX A

The rate constants and the equilibrium constants used in the rate equations [R_1-R_{16}]:

$$k_1 = k_{0,1}\exp\left(\frac{-E_1}{RT}\right) = 0.46\exp\left(\frac{-22000}{RT}\right) \quad (A.1)$$

$$k_2 = k_{0,2}\exp\left(\frac{-E_2}{RT}\right) = 20.6\exp\left(\frac{-99000}{RT}\right) \quad (A.2)$$

$$k_3 = k_{0,3}\exp\left(\frac{-E_3}{RT}\right) = (4.21\times10^{3})\exp\left(\frac{-127000}{RT}\right) \quad (A.3)$$

$$k_4 = k_{0,4}\exp\left(\frac{-E_4}{RT}\right) = (6.21\times10^{21})\exp\left(\frac{-29000\times4.184}{RT}\right)/(60\times100^{6}) \quad (A.4)$$

$$k_5 = k_{0,5}\exp\left(\frac{-E_5}{RT}\right) = 4.66\exp\left(\frac{-77416}{RT}\right) \quad (A.5)$$

$$k_6 = k_{0,6}\exp\left(\frac{-E_6}{RT}\right) = (1.31\times10^{-4})\exp\left(\frac{-26413}{RT}\right) \quad (A.6)$$

$$k_7 = k_{0,7}\exp\left(\frac{-E_7}{RT}\right) = (1.097\times10^{-4})\exp\left(\frac{-26505}{RT}\right) \quad (A.7)$$

$$k_8 = k_{0,8}\exp\left(\frac{-E_8}{RT}\right) = (4.18\times10^{-3})\exp\left(\frac{-23666}{RT}\right) \quad (A.8)$$

$$k_9 = k_{0,9}\exp\left(\frac{-E_9}{RT}\right) = (1.17 \times 10^{15})\exp\left(\frac{-240100}{RT}\right) \quad (A.9)$$

$$k_{10} = k_{0,10}\exp\left(\frac{-E_{10}}{RT}\right) = (5.43 \times 10^{5})\exp\left(\frac{-67130}{RT}\right) \quad (A.10)$$

$$k_{11} = k_{0,11}\exp\left(\frac{-E_{11}}{RT}\right) = (2.83 \times 10^{14})\exp\left(\frac{-243900}{RT}\right) \quad (A.11)$$

$$K_I = \exp\left(\frac{-26830}{T_s} + 30.114\right) \quad (A.12)$$

$$K_{II} = \exp\left(\frac{4400}{T_s} - 4.036\right) \quad (A.13)$$

$$K_{III} = K_I K_{II} \quad (A.14)$$

$$\Omega = 1 + K_{CO}p_{CO} + K_{H_2}p_{H_2} + K_{CH_4}p_{CH_4} + K_{H_2O}\frac{p_{H_2O}}{p_{H_2}} \quad (A.15)$$

$$K_i = K_{oi}\exp\left(\frac{-\Delta H_i}{R_g T}\right) \quad (A.16)$$

$$k_{12} = k_{0,12}\exp\left(\frac{-E_{12}}{RT}\right) = 0.207\exp\left(\frac{-9920}{RT}\right) \quad (A.17)$$

$$K_{CO2} = (2.4 \times 10^{-3})\exp\left(\frac{77500}{RT}\right) \quad (A.18)$$

$$k_{13} = k_{0,13}\exp\left(\frac{-E_{13}}{RT}\right) = 43.4\exp\left(\frac{-58900}{RT}\right) \quad (A.19)$$

$$K_{p,d} = \exp\left(\frac{104}{R}\right) \times \exp\left(\frac{-88400}{RT}\right) \quad (A.20)$$

$$K_{CH4,d} = (2.1 \times 10^{-6})\exp\left(\frac{78000}{RT}\right) \quad (A.21)$$

$$K_{r,d} = (5.18 \times 10^{7})\exp\left(\frac{-133000}{RT}\right) \quad (A.22)$$

$$k_{14} = k_{0,14}\exp\left(\frac{-E_{14}}{RT}\right) = (3.08 \times 10^{4})\exp\left(\frac{-166000}{RT}\right) \quad (A.23)$$

$$K_{H2O,g} = (4.73 \times 10^{-6})\exp\left(\frac{97700}{RT}\right) \quad (A.24)$$

$$K_{CH4,g} = 3.49 \quad (A.25)$$

$$K_{r,g} = (1.83 \times 10^{13}) \exp\left(\frac{-216000}{RT}\right) \quad (A.26)$$

$$K_{p,g} = \exp\left(\frac{137}{R}\right) \exp\left(\frac{-126000}{RT}\right) \quad (A.27)$$

$$k_{15} = k_{0,15}\exp\left(\frac{-E_{15}}{RT}\right) = (8.37 \times 10^{10}) \exp\left(\frac{-312000}{RT}\right) \quad (A.28)$$

$$K_{CO,g} = (37.8 \times 10^{-6}) \exp\left(\frac{100000}{RT}\right) \quad (A.29)$$

$$K_{CO2,g} = (8.17 \times 10^{7}) \exp\left(\frac{-104000}{RT}\right) \quad (A.30)$$

$$K_{p,g,CO2} = \exp\left(\frac{178}{R}\right) \exp\left(\frac{-169000}{RT}\right) \quad (A.31)$$

$$\frac{dq_{CO2}}{dt} = k_{carb}(X_{max} - X)(\upsilon_{CO2} - \upsilon_{CO2,eq}) \quad (A.32)$$

$$\upsilon_{CO2,eq} = (4.137 \times 10^{7})\exp\left(\frac{-20474}{T}\right) \quad (A.33)$$

APPENDIX B

Axial mass dispersion coefficient is given as[57];

$$D_z = 0.73D_m + \frac{0.5u_s d_p}{1 + 9.49D_m/u_s d_p} \quad (B.1)$$

Here 'D_z' is the axial dispersion coefficient and measure in m^2/s. 'd_p' is the diameter of particle, 'u_s' is the interstitial gas velocity and 'D_m' is the average molecular diffusivity.

Effective thermal conductivity is given in following relations[58];

$$\frac{\lambda_z^f}{\lambda_g} = \frac{\lambda_z^o}{\lambda_g} + 0.75PrRe_p \quad (B.2)$$

Here,

$$\frac{\lambda_z^o}{\lambda_g} = \varepsilon_b + \frac{1 - \varepsilon_b}{0.139\varepsilon_b - 0.0339 + \left(\frac{2}{3}\right)\lambda_g/\lambda_s} \quad (B.3)$$

Where 'λ_g' is the average thermal conductivity of gas and 'λ_s' is the average thermal conductivity of solid material. Relation for mass transfer coefficient is given as[59];

$$k_{g,i} = j_{D,i} Re Sc_i^{1/3} \frac{D_i}{d_p} \quad (B.4)$$

Also,

$$\varepsilon_b j_{D,i} = 0.765 Re^{-0.82} + 0.365 Sc_i^{-0.398} \quad (B.5)$$

Dimensionless numbers are given as,

$$Re = \frac{\rho_f u_s d_p}{\mu} \quad ; \quad 0.01 < Re < 1500 \quad (B.6)$$

$$Sc_i = \frac{\mu}{\rho_f D_i} \quad ; \quad 0.6 < Sc < 7000 \ , \ 0.25 < \varepsilon_b < 0.96 \quad (B.7)$$

Similarly to find out the heat transfer coefficient and its dimensional numbers following relations are used in the model formulation[59, 60];

$$h_f = j_H \frac{C_{pg} G_s}{Pr^{2/3}} \quad (B.8)$$

Here,

$$j_H = 0.91 Re^{-0.51} \psi \quad ; \quad 0.01 < Re < 50 \quad (B.9)$$

$$j_H = 0.61 Re^{-0.41} \psi \quad ; \quad 50 < Re < 1000 \quad (B.10)$$

$$Pr = \frac{C_{pg} \mu_g}{\lambda_g} \quad (B.11)$$

APPENDIX C

$C_{i,in}$[mol m^{-3}] Where;i = CH_4, CO, H_2, H_2O, CO_2 and N_2	[74.2, 0, 0.42, 222.5, 0, 74.2]
$C_{i,o}$ [mol m^{-3}]	0
P_{in} [bar]	30
T_{in} [K]	973.15
T_o [K]	973.15

$T_{s,in}$ [K]	973.15
$T_{s,o}$ [K]	973.15

Table C: The values of initial and boundary conditions

REFERENCES

[1] M.R. Allen, J.F.B. Mitchell, P.A. Stott, Test of a decadal climate forecast, Nature Geoscience, 6 (2013) 243-244.

[2] F.-X. Chiron, G.S. Patience, S. Rifflart, Hydrogen production through chemical looping using NiO/NiAl2O4 as oxygen carrier, Chemical Engineering Science, 66 (2011) 6324-6330.

[3] R.B. Gupta, Hydrogen fuel: production, transport, and storage, Crc Press, 2008.

[4] R. Cortright, R. Davda, J. Dumesic, Hydrogen from catalytic reforming of biomass-derived hydrocarbons in liquid water, Nature, 418 (2002) 964-967.

[5] C.H. Bartholomew, R.J. Farrauto, Fundamentals of industrial catalytic processes, John Wiley & Sons, 2011.

[6] G.-h. Xiu, P. Li, A.E. Rodrigues, Sorption-enhanced reaction process with reactive regeneration, Chemical Engineering Science, 57 (2002) 3893-3908.

[7] D.P. Harrison, Sorption-enhanced hydrogen production: a review, Industrial & engineering chemistry research, 47 (2008) 6486-6501.

[8] B. Dou, V. Dupont, G. Rickett, N. Blakeman, P.T. Williams, H. Chen, Y. Ding, M. Ghadiri, Hydrogen production by sorption-enhanced steam reforming of glycerol, Bioresource Technology, 100 (2009) 3540-3547.

[9] Z. Yong, V. Mata, A.r.E. Rodrigues, Adsorption of carbon dioxide at high temperature—a review, Separation and Purification Technology, 26 (2002) 195-205.

[10] E. Ochoa-Fernández, G. Haugen, T. Zhao, M. Rønning, I. Aartun, B. Børresen, E. Rytter, M. Rønnekleiv, D. Chen, Process design simulation of H2 production by sorption enhanced steam methane reforming: evaluation of potential CO2 acceptors, Green Chemistry, 9 (2007) 654-662.

[11] J.C. Abanades, The maximum capture efficiency of CO2 using a carbonation/calcination cycle of CaO/CaCO 3, Chemical Engineering Journal, 90 (2002) 303-306.

[12] V. Dupont, A. Ross, E. Knight, I. Hanley, M. Twigg, Production of hydrogen by unmixed steam reforming of methane, Chemical Engineering Science, 63 (2008) 2966-2979.

[13] D. Alvarez, J.C. Abanades, Determination of the critical product layer thickness in the reaction of CaO with CO2, Industrial & engineering chemistry research, 44 (2005) 5608-5615.

[14] A. Silaban, M. Narcida, D. Harrison, Characteristics of the reversible reaction between CO2 (g) and calcined dolomite, Chemical Engineering Communications, 146 (1996) 149-162.

[15] J. Blamey, V. Manovic, E.J. Anthony, D.R. Dugwell, P.S. Fennell, On steam hydration of CaO-based sorbent cycled for CO 2 capture, Fuel, 150 (2015) 269-277.

[16] S. Wu, T. Beum, J. Yang, J. Kim, Properties of Ca-base CO2 sorbent using Ca (OH)2 as precursor, Industrial & engineering chemistry research, 46 (2007) 7896-7899.

[17] P. Pimenidou, G. Rickett, V. Dupont, M.V. Twigg, High purity H2 by sorption-enhanced chemical looping reforming of waste cooking oil in a packed bed reactor, Bioresource Technology, 101 (2010) 9279-9286.

[18] R.A. Molinder, CO2 capture materials for sorption enhanced steam reforming, in, University of Leeds, 2012.

[19] A. Solieman, J. Dijkstra, W. Haije, P. Cobden, R. van den Brink, Calcium oxide for CO2 capture: Operational window and efficiency penalty in sorption-enhanced steam methane reforming, International Journal of Greenhouse Gas Control, 3 (2009) 393-400.

[20] R. Lyon, Methods and systems for heat transfer by unmixed combustion using mixed catalysts, in: Fuel and Energy Abstracts, 1997, pp. 108.

[21] R.K. Lyon, J.A. Cole, Unmixed combustion: an alternative to fire, Combustion and Flame, 121 (2000) 249-261.

[22] R.V. Kumar, J.A. Cole, R.K. Lyon, Unmixed reforming: an advanced steam reforming process, in: Preprints of Symposia, 218th. ACS National Meeting, August, 1999, pp. 22-26.

[23] R.K. Lyon, J.A. Cole, Unmixed combustion: an alternative to fire, Combustion and Flame, 121 (2000) 249-261.

[24] G. Rizeq, J. West, A. Frydman, R. Subia, V. Zamansky, K. Das, Advanced Gasification-Combustion Technology for Production of Hydrogen, Power and Sequestration-Ready CO2, in: GE Global Research, US DOE NETL, Gasification Technologies Conference, 2003.

[25] N.a.E.R.G. Warren K. Lewis, Production of pure carbon dioxide, (1950).

[26] H. Richter, K. Knoche, Reversibility of Combustion Proceases, Efficiency and Costing, Second Law Analysis of Processes, in: Gaggioli R A. ACS Symposium Series, pp. 1983.1971-1985.

[27] M. Ishida, D. Zheng, T. Akehata, Evaluation of a chemical-looping-combustion power-generation system by graphic exergy analysis, Energy, 12 (1987) 147-154.

[28] Q. Zafar, T. Mattisson, B. Gevert, Integrated hydrogen and power production with CO2 capture using chemical-looping reforming redox reactivity of particles of CuO, Mn2O3, NiO, and Fe2O3 using SiO2 as a support, Industrial & engineering chemistry research, 44 (2005) 3485-3496.

[29] L.F. de Diego, P. Gayán, J. Celaya, J.M. Palacios, J. Adánez, Operation of a 10kWth chemical-looping combustor during 200h with a CuO–Al2 O3 oxygen carrier, Fuel, 86 (2007) 1036-1045.

[30] R.V. Kumar, R.K. Lyon, J.A. Cole, Unmixed Reforming: A Novel Autothermal Cyclic Steam Reforming Process, in: Advances in Hydrogen Energy, Springer, 2002, pp. 31-45.

[31] M. Rydén, P. Ramos, H2 production with CO2 capture by sorption enhanced chemical-looping reforming using NiO as oxygen carrier and CaO as CO2 sorbent, Fuel Processing Technology, 96 (2012) 27-36.

[32] M. Rydén, P. Ramos, H 2 production with CO2 capture by sorption enhanced chemical-looping reforming using NiO as oxygen carrier and CaO as CO2 sorbent, Fuel Processing Technology, 96 (2012) 27-36.

[33] P. Kulkarni, J. Guan, R. Subia, Z. Cui, J. Manke, A. Frydman, W. Wei, R. Shisler, R. Ayala, G. Rizeq, Fuel-Flexible Gasification-Combustion Technology for Production of H2 and Sequestration-Ready CO2, in, GE Energy & Environmental Research Corporation, 2008.

[34] B. Monnerat, L. Kiwi-Minsker, A. Renken, Hydrogen production by catalytic cracking of methane over nickel gauze under periodic reactor operation, Chemical Engineering Science, 56 (2001) 633-639.

[35] D.K. Lee, I.H. Baek, W.L. Yoon, Modeling and simulation for the methane steam reforming enhanced by in situ CO2 removal utilizing the CaO carbonation for H2 production, Chemical Engineering Science, 59 (2004) 931-942.

[36] I. Iliuta, R. Tahoces, G.S. Patience, S. Rifflart, F. Luck, Chemical-looping combustion process: Kinetics and mathematical modeling, AIChE Journal, 56 (2010) 1063-1079.

[37] A. Antzara, E. Heracleous, D.B. Bukur, A.A. Lemonidou, Thermodynamic analysis of hydrogen production via chemical looping steam methane reforming coupled with in situ CO2 capture, International Journal of Greenhouse Gas Control, 32 (2015) 115-128.

[38] B.M. Corbella, L.F. de Diego, F. García-Labiano, J. Adánez, J.M. Palacios, Characterization study and five-cycle tests in a fixed-bed reactor of titania-supported nickel oxide as oxygen carriers for the chemical-looping combustion of methane, Environmental science & technology, 39 (2005) 5796-5803.

[39] C. Dueso, M. Ortiz, A. Abad, F. García-Labiano, F. Luis, P. Gayán, J. Adánez, Reduction and oxidation kinetics of nickel-based oxygen-carriers for chemical-looping combustion and chemical-looping reforming, Chemical engineering journal, 188 (2012) 142-154.

[40] T.J. Keskitalo, K.J. Lipiäinen, A.O.I. Krause, Kinetic modeling of coke oxidation of a ferrierite catalyst, Industrial & engineering chemistry research, 45 (2006) 6458-6467.

[41] B. Subramaniam, A. Varma, Reaction kinetics on a commercial three-way catalyst: the carbon monoxide-nitrogen monoxide-oxygen-water system, Industrial & engineering chemistry product research and development, 24 (1985) 512-516.

[42] Z. Zhou, L. Han, G.M. Bollas, Model-based analysis of bench-scale fixed-bed units for chemical-looping combustion, Chemical Engineering Journal, 233 (2013) 331-348.

[43] P. Kolbitsch, T. Pröll, H. Hofbauer, Modeling of a 120kW chemical looping combustion reactor system using a Ni-based oxygen carrier, Chemical Engineering Science, 64 (2009) 99-108.

[44] M.M. Hossain, H.I. de Lasa, Reactivity and stability of Co-Ni/Al2O3 oxygen carrier in multicycle CLC, AIChE Journal, 53 (2007) 1817-1829.

[45] H. Jin, M. Ishida, Reactivity study on natural-gas-fueled chemical-looping combustion by a fixed-bed reactor, Industrial & engineering chemistry research, 41 (2002) 4004-4007.

[46] M. Rydén, A. Lyngfelt, T. Mattisson, Synthesis gas generation by chemical-looping reforming in a continuously operating laboratory reactor, Fuel, 85 (2006) 1631-1641.

[47] F. Luis, M. Ortiz, J. Adánez, F. García-Labiano, A. Abad, P. Gayán, Synthesis gas generation by chemical-looping reforming in a batch fluidized bed reactor using Ni-based oxygen carriers, Chemical Engineering Journal, 144 (2008) 289-298.

[48] F. Luis, M. Ortiz, F. García-Labiano, J. Adánez, A. Abad, P. Gayán, Hydrogen production by chemical-looping reforming in a circulating fluidized bed reactor using Ni-based oxygen carriers, Journal of Power sources, 192 (2009) 27-34.

[49] T. Mattisson, M. Johansson, A. Lyngfelt, The use of NiO as an oxygen carrier in chemical-looping combustion, Fuel, 85 (2006) 736-747.

[50] J. Xu, G.F. Froment, Methane steam reforming, methanation and water-gas shift: I. Intrinsic kinetics, AIChE Journal, 35 (1989) 88-96.

[51] M. Halabi, M. De Croon, J. Van der Schaaf, P. Cobden, J. Schouten, Modeling and analysis of autothermal reforming of methane to hydrogen in a fixed bed reformer, Chemical Engineering Journal, 137 (2008) 568-578.

[52] J. Feick, D. Quon, Mathematical models for the transient behavior of a packed bed reactor, The Canadian Journal of Chemical Engineering, 48 (1970) 205-211.

[53] S. Bhatia, D. Perlmutter, Effect of the product layer on the kinetics of the CO2-lime reaction, AIChE Journal, 29 (1983) 79-86.

[54] J. Fernandez, J. Abanades, R. Murillo, Modeling of sorption enhanced steam methane reforming in an adiabatic fixed bed reactor, Chemical Engineering Science, 84 (2012) 1-11.

[55] B. Monnerat, L. Kiwi-Minsker, A. Renken, Mathematical modelling of the unsteady-state oxidation of nickel gauze catalysts, Chemical Engineering Science, 58 (2003) 4911-4919.

[56] J. Rostrup-Nielsen, J. Sehested, J.K. Nørskov, Hydrogen and synthesis gas by steam-and CO2 reforming, in: Advances in Catalysis, 2002.

[57] M. Edwards, J. Richardson, Gas dispersion in packed beds, Chemical Engineering Science, 23 (1968) 109-123.

[58] S. Yagi, D. Kunii, N. Wakao, Studies on axial effective thermal conductivities in packed beds, AIChE Journal, 6 (1960) 543-546.

[59] C.J. Geankoplis, Transport processes and unit operations, (1993).

[60] D. Handley, P.J. Heggs, The effect of thermal conductivity of the packing material on transient heat transfer in a fixed bed, International Journal of Heat and Mass Transfer, 12 (1969) 549-570.